

UNCLASSIFIED

AD NUMBER
ADC000488
CLASSIFICATION CHANGES
TO
unclassified
FROM
confidential
AUTHORITY
31 Dec 1982 per document marking

THIS PAGE IS UNCLASSIFIED

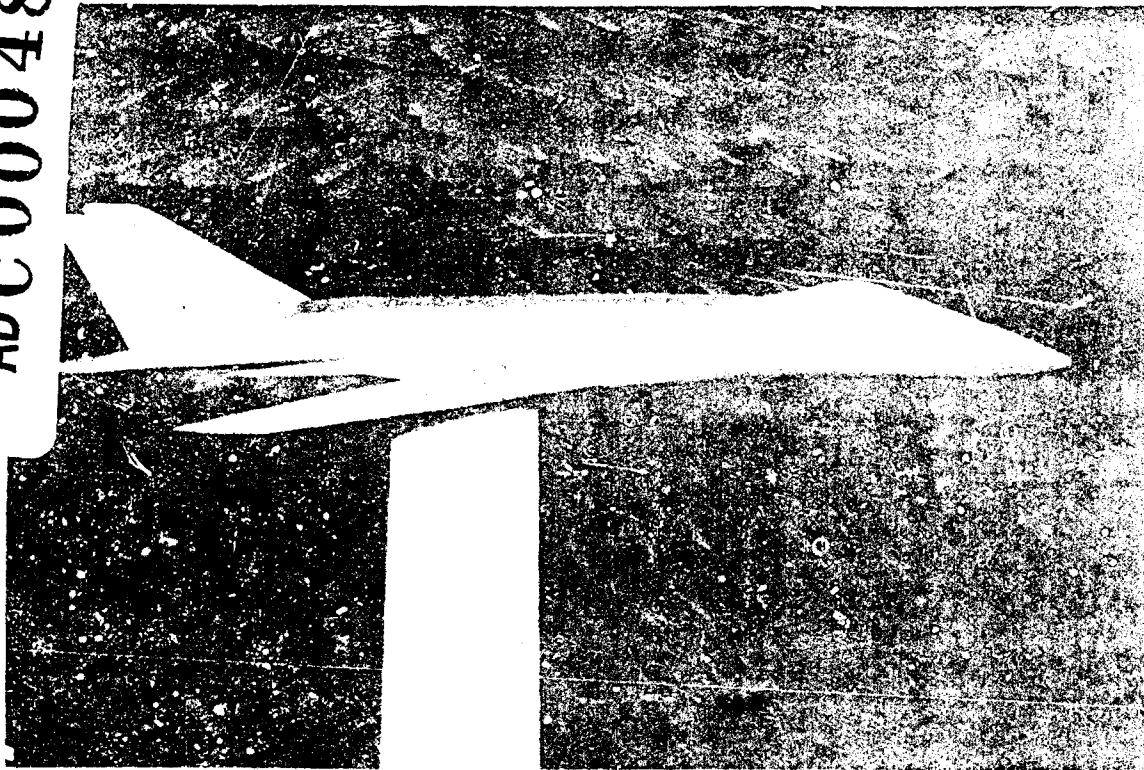
UNCLASSIFIED

AD NUMBER
ADC000488
CLASSIFICATION CHANGES
TO
confidential
FROM
secret
AUTHORITY
Jun 1976 per GDS document marking

THIS PAGE IS UNCLASSIFIED

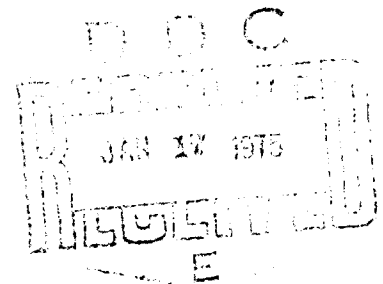
~~SECRET~~

ADC 000488



DESIGN OF AIRCRAFT FOR LOW RADAR CROSS
SECTION - BROADSIDE SECTOR (U)
VOLUME I

D180-17939-1



RESEARCH & ENGINEERING DIVISION
BOEING AEROSPACE COMPANY
SEATTLE, WASHINGTON

~~SECRET~~

~~SECRET~~

ISSUE No. *67*

D180-17939-1

ANNUAL TECHNICAL REPORT

DESIGN OF AIRCRAFT FOR LOW RADAR CROSS SECTION - BROADSIDE SECTOR (U) VOLUME I

June 1974

PREPARED FOR:
THE OFFICE OF NAVAL RESEARCH
AERONAUTICS PROGRAMS
ARLINGTON, VIRGINIA
CONTRACT N00014 72-C 0303/NR212-220

SECRET CLASSIFIED BY:
DIRECTOR, NAVAL APPLICATIONS & ANALYSIS DIVISION
SUBJECT TO GENERAL DECLASSIFICATION SCHEDULE
OF EXECUTIVE ORDER 11652. AUTOMATICALLY DOWN
GRADED AT TWO YEAR INTERVALS & DECLASSIFIED ON
31 DECEMBER 1982

"REPRODUCTION IN WHOLE OR IN PART IS PERMITTED FOR ANY
PURPOSE OF THE UNITED STATES GOVERNMENT."

NATIONAL SECURITY INFORMATION
UNAUTHORIZED DISCLOSURE
SUBJECT TO CRIMINAL SANCTIONS

RESEARCH & ENGINEERING DIVISION
BOEING AEROSPACE COMPANY
(A DIVISION OF THE BOEING COMPANY)
SEATTLE, WASHINGTON 98124

DDC
RECEIVED
JAN 17 1975
REGULATED
E

DDC CONTROL
NO. 50040

~~SECRET~~

Unclassified

~~SECRET~~

SECURITY CLASSIFICATION OF THIS PAGE (When Data Entered)

REPORT DOCUMENTATION PAGE		READ INSTRUCTIONS BEFORE COMPLETING FORM
1. REPORT NUMBER D180-17939-1	2. GOVT ACCESSION NO.	3. RECIPIENT'S CATALOG NUMBER
4. TITLE (and Subtitle) Design of Aircraft for Low Radar Cross Section Broadside Sector. Volume I		5. TYPE OF REPORT & PERIOD COVERED Annual - 1973
7. AUTHOR(s) J. D. Kelly G. A. Taylor		6. PERFORMING ORG. REPORT NUMBER
8. PERFORMING ORGANIZATION NAME AND ADDRESS Boeing Aerospace Company Seattle, Washington 98124		8. CONTRACT OR GRANT NUMBER(s) N00014-72-C-0303
11. CONTROLLING OFFICE NAME AND ADDRESS Office of Naval Research Arlington, Virginia 22217		10. PROGRAM ELEMENT, PROJECT, TASK AREA & WORK UNIT NUMBERS NR 212-220
14. MONITORING AGENCY NAME & ADDRESS (if different from Controlling Office)		12. REPORT DATE June, 1974
		13. NUMBER OF PAGES 72
		15. SECURITY CLASS. (of this report) Secret
		15a. DECLASSIFICATION/DOWNGRADING SCHEDULE GDS - Ex. Order 11652
16. DISTRIBUTION STATEMENT (of this Report) Qualified requestors may obtain a copy of this report from DDC.		
17. DISTRIBUTION STATEMENT (of the abstract entered in Block 20, if different from Report) -		
18. SUPPLEMENTARY NOTES -		
19. KEY WORDS (Continue on reverse side if necessary and identify by block number) Radar Cross Section Broadside Sector Traveling Waves		
20. ABSTRACT (Continue on reverse side if necessary and identify by block number) This study was designed to develop an understanding of the composition of the RCS scattered in the broadside sector. Parametric studies were made to determine the averaged RCS of the broadside sector for various combinations of fuselage shape, wing shape and locations and empennage geometries. The fuselage shapes were circular, triangular, square and		

DD FORM 1 JAN 73 1473

EDITION OF 1 NOV 65 IS OBSOLETE

UNCLASSIFIED

SECURITY CLASSIFICATION OF THIS PAGE (When Data Entered)

(This page is unclassified)

~~SECRET~~

UNCLASSIFIED

D180-17939-1

SECURITY CLASSIFICATION OF THIS PAGE(When Data Entered)

20. elliptical. Subsonic and supersonic wings were combined
Cont. with the fuselage at three different locations, top,
center and flush with the bottom line of the fuselage.
The RCS of the broadside sector was also determined
for three tail geometries, T-tail, V-tail and twin
tail.

An airplane with a low RCS in the broadside sector
was designed based on the design guideline data obtained
from the parametric study.

UNCLASSIFIED

SECURITY CLASSIFICATION OF THIS PAGE(When Data Entered)

UNCLASSIFIED

D180-17939-1

FOREWORD (U)

- (U) The research described in this report was conducted under contract #N0C014-72-C-0303 sponsored by the Office of Naval Research (ONR), Naval Applications and Analysis Division Code 461. Program Manager is G. A. Heffernan, Capt. USN and the Technical Monitor is Mr. D. S. Siegel.
- (U) This Annual Technical Report discusses research performed during the calendar year 1973. Volume I contains the program details, conclusions, and recommendations. Volume II of this report contains the unclassified RCS data calculated for the various airplane configurations studied. Previous research conducted during 1972 is described in a preceding Annual Technical Report #D180-14192-1, The Boeing Company, 1973, Secret. All research under this contract has been conducted within The Boeing Aerospace Company, Research and Engineering Division. The program management is the responsibility of Mr. J. D. Kelly. The program technical leader is Mr. G. A. Taylor and the principal technical investigator is Mr. W. S. Hammond.

UNCLASSIFIED

UNCLASSIFIED

D180-17939-1

Table of Contents (U)

		<u>Page</u>
1.0	Introduction	1
2.0	Summary	4
3.0	Technical Approach	13
3.1	Methodology	13
3.2	Design Guideline Data	39
4.0	Design Guideline Application	53
4.1	Low RCS Aircraft Design Selection	53
4.2	"Low RCS Airplane" Model Tests	53
5.0	Conclusions and Recommendations	60
6.0	References	62

UNCLASSIFIED

D180-17939-1

List of Figures

<u>Figure</u>	<u>Title</u>	<u>Page</u>
2-1	Fuselage Shapes (U)	5
2-2	Computed RCS - Triangular Body - Bottom Supersonic Wing - 12 GHz (U)	7
3-1	Supersonic HIPASS Airplane (U)	14
3-2	Circular Fuselage Model (U)	15
3-3	Definition of Wing to the Computer (U)	17
3-4	Empennage Geometry (U)	19
3-5	Measured RCS - Circular Model (U)	20
3-6	Measured RCS - Circular Model with Fairings (U)	21
3-7	Computed RCS Circular Model - 32 GHz (U)	23
3-8	Measured RCS - Circular Model (U)	24
3-9	Measured RCS - Circular Model Measure- ments (U)	25
3-10	Flat Plate RCS (U)	29
3-11	Traveling Wave Reflection Coefficient (U)	30
3-12	Traveling Wave RCS (U)	32
3-13	Traveling Wave Reflection vs Radius of Curvature (U)	33
3-14	Absorber Test Fixture	36
3-15	Absorber Test Specimens	37
3-16	Absorber Performance - 3 GHz	38
3-17	Computed RCS - Circular Body - Center Subsonic Wing - 4 GHz (U)	40
3-18	Computed RCS - Triangular Body - Center Subsonic Wing - 4 GHz (U)	41
3-19	Computed RCS - Square Body - Center Subsonic Wing - 4 GHz (U)	42
3-20	Computed RCS - Elliptical Body - Center Subsonic Wing - 4 GHz (U)	43
4-1	Low RCS Airplane (U)	54
4-2	Measured RCS - Low RCS Airplane (U)	56
4-3	Measured RCS - Low RCS Airplane Model (U)	57
4-4	RCS Contour - Low RCS Airplane (U)	58
4-5	RCS Contour - Low RCS Airplane (U)	59

UNCLASSIFIED

D180-17939-1

List of Tables

<u>Table</u>	<u>Title</u>	<u>Page</u>
2.1	RCS - Upper Broadside Sector (U)	8
2.2	RCS - Lower Broadside Sector (U)	9
2.3	RCS - Entire Broadside Sector (U)	10
2.4	Empennage Comparison (U)	10a
3.1	Fuselage Shape Effects - Centered Subsonic Wing (U)	45
3.2	Wing Location Effects - Circular Fuselage (U)	46
3.3	Wing Location Effects - Triangular Fuselage (U)	47
3.4	Wing Sweep Effects - Center Location (U)	49
3.5	Wing Sweep Effects - Bottom Location (U)	50
3.6	Empennage Effects (U)	52

~~CONFIDENTIAL~~

D180-17939-1

1.0 INTRODUCTION (U)

(U)The survival of any military aircraft designed to operate against radar guided threats, will be influenced by the aircraft radar cross section (RCS). The probability of aircraft survival against a given radar guided threat will be determined by several factors including: speed, altitude, tactics and active electronic countermeasures (jammers, chaff, decoys). The degree of improvement in survivability resulting from use of any of these techniques will be influenced by the aircraft RCS. The lower the RCS the more effective a given defensive measure becomes. Obviously, there is a limit to the degree of RCS control which is both practical and desirable. This level of RCS is unique to a given aircraft weapon system. However, in order to achieve an optimum survivability and at the same time an efficient cost and weight position, the aircraft RCS should be specified and controlled from the beginning of the system design process.

(U)The design of methods for control of the radar cross section of aircraft has primarily centered about the forward sector, nominally $\pm 60^\circ$ from nose-on. The similar angular sector about tail-on has received secondary attention and the broadside sector has received the least attention from a RCS viewpoint. The de-emphasizing of broadside RCS is a result of two major considerations: 1) the operational factors which have shown that broadside exposure to most threats is very small and 2) the large broadside sector RCS values of "typical" aircraft are, to a large extent, unmanageable from an RCS viewpoint. Current operational aircraft will typically have RCS values ranging upward from hundreds to thousands of square meters in the broadside sector, ($\pm 30^\circ$ in azimuth and elevation about aircraft broadside). However, recent advances in Soviet missile technology have shown that the broadside sector RCS can be significant to aircraft survival. The improved speed, range and maneuverability of Soviet surface-to-air and air-to-air missiles are such that a broadside shot is feasible for all but extremely fast targets. This potential threat capability has created an increasing interest in the control of aircraft RCS throughout the viewing sector including the broadside region.

~~CONFIDENTIAL~~

~~CONFIDENTIAL~~

D180-17939-1

(C)The control of the RCS of aircraft has been the subject of interest in the study reported here and in two preceding studies sponsored by the Office of Naval Research with The Boeing Company.^{1,2} These three studies have shown the following:

- 1) An advanced fighter-attack aircraft can be designed for extremely low RCS throughout the entire threat sector with no major cost or performance penalties.
- 2) The control of details along the airframe, particularly control surfaces, is essential to the design of aircraft to low levels of RCS (below 1 square meter) in the forward and aft sectors.
- 3) Control of the aircraft configuration can provide for a low RCS (below ten square meters) in the broadside sector.

(U)The last of the above results is the subject of this report. The research conducted during this recent program as well as the two preceding studies is designed to provide a fundamental understanding of the RCS characteristics of aircraft. This latest study has developed generalized aircraft RCS trend data in the broadside sector. This data provides preliminary design guidelines for selection of a basic aircraft configuration to satisfy RCS requirements over the broadside sector.

(U)A special class of electromagnetic waves, traveling waves, are also included in the studies. The influence of traveling waves on RCS in the broadside sector is shown to be significant for low RCS levels (below 10 square meters) and means for estimating the traveling wave RCS contributions are presented.

~~CONFIDENTIAL~~

~~CONFIDENTIAL~~

DL80-17939-1

(U)The use of radar absorbing material (RAM) to achieve a low RCS over the broadside sector has not been emphasized during this study. The installation of RAM as an integral part of the aircraft surface will result in a reduction in RCS in a straight-forward manner. However, the installation of a variety of materials such as RAM, as part of an airframe surface can result in substantial increases in the forward and aft sector RCS. Furthermore, the use of absorbers, without control of the airframe configuration, is not an efficient means of control of aircraft RCS and, therefore, will result in unwarranted weight and cost increases. Therefore, absorbers are considered for use only as a last resort for control of broadside RCS. For this study, configuration control is to be emphasized.

(U)The effectiveness of configuration selection as a means of broadside RCS control is demonstrated during this program from RCS measurements on a test model of a "Low RCS Airplane" designed to exhibit RCS control over the lower hemisphere. This airplane was developed as a practical concept for an advanced fighter-attack airplane using present technology.

~~(c)~~The results of this program serve to further substantiate, that RCS control is a realizable aircraft design feature and that the problems associated with RCS control are solvable within today's technology. Failure to include RCS control where required for advanced weapon systems, will result in less effective systems from cost, weight or survivability standpoints. RCS control can be used in concert with active electronic counter-measures (ECM) to provide an optimum survivability at minimum weight and cost. The use of active ECM alone is not, in general, the most cost effective means for achieving system survivability or penetrability. Furthermore, there are instances where available ECM systems do not have sufficient power to adequately protect aircraft without RCS control.³

(U)The results of this program are summarized in Section 2.0 of this report and the detailed program results are described in Section 3.0. The application of broadside RCS control to the "Low RCS Airplane" is the subject of Section 4.0. The conclusions and recommendations resulting from this study are summarized in Section 5.0 and pertinent references are listed in Section 6.0.

~~CONFIDENTIAL~~

UNCLASSIFIED

D180-17939-1

2.0 SUMMARY (U)

(U)The primary objective of this study is to develop a fundamental understanding of the contributors to aircraft RCS in the broadside sector. This is done through a combined theoretical and empirical approach. The RCS of a variety of representative aircraft configurations are computed using a computer program employing a modified geometric optics approach. These computations are verified by a comparison with experimental RCS data taken on a test model. The traveling wave contributions to the broadside sector RCS are calculated from expressions derived from empirical data. A set of design guideline data was then prepared which illustrates the trends in broadside RCS as a function of the airplane configuration. In addition, preliminary assessment is made of the contributions to broadside RCS from traveling waves as well as from specular reflections. These design data are applied to a configuration which exhibits a low RCS in the lower hemisphere. RCS measurements on a test model of the final configuration verify the low RCS values estimated.

(U)The design guideline RCS data relating to specular type reflections was obtained from computer calculations on airplane configurations employing various fuselage and empennage geometries and different wing locations and sweep angles. Fuselage geometries studied were circular, elliptical, square and triangular. These are illustrated in Figure 2.1. The fuselages were all designed for constant volume. The empennage geometries studied were the T-tail, V-tail, and tilted twin tail arrangements. Top, center and bottom wing locations with typical subsonic and supersonic sweep angles were also included. The RCS for all of the configurations was computed over the sector $\pm 30^\circ$ in azimuth about broadside and at roll angles of $+30, +20, +10, 0, -10, -20$, and -30 degrees. The plus angles correspond to viewing the aircraft from above. The calculated RCS includes only the electromagnetic energy reflected in a quasioptical manner (specular and double reflections). Additional RCS contributions are present due to traveling wave reflections. These RCS contributions are examined separately.

D180-17939-1
UNCLASSIFIED

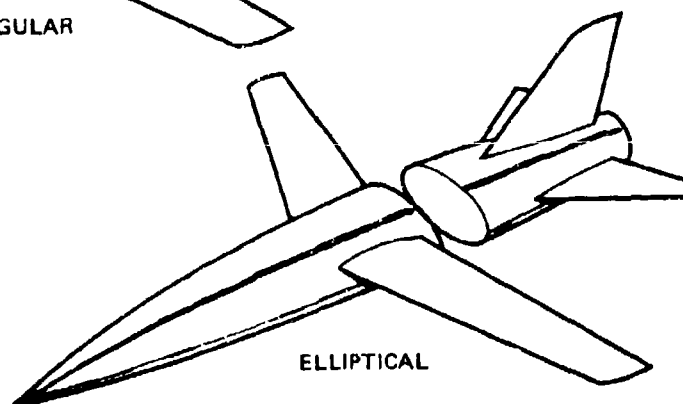
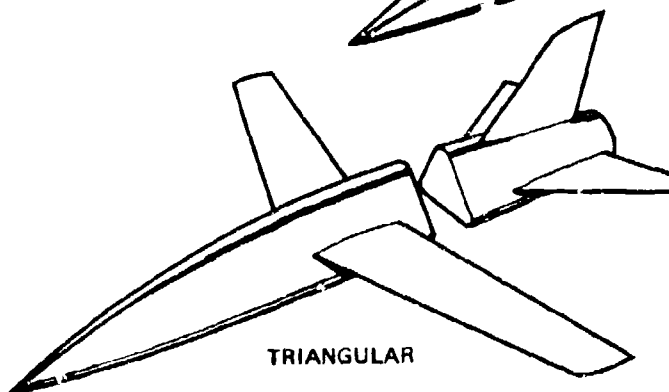
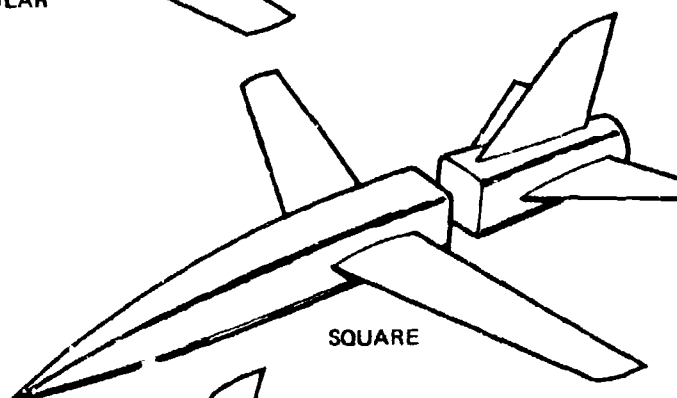
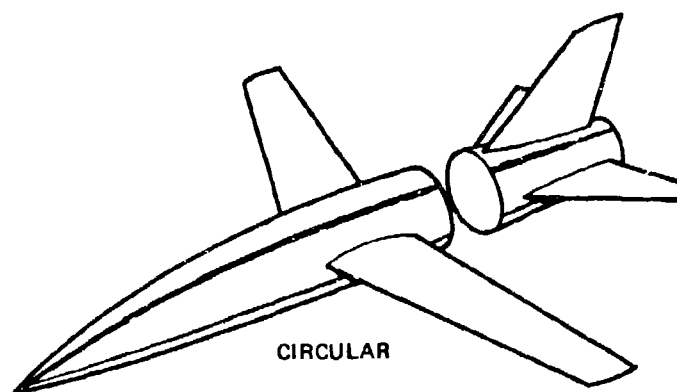


Figure 2-1: Fuselage Shapes (U)

UNCLASSIFIED

D180-17939-1

(U) The average RCS over a ten degree azimuth interval was computed at each ten degree azimuth angle (0° , $+10^\circ$, $+20^\circ$ and $+30^\circ$ from broadside) for the various aircraft geometries studied. This computation was repeated for each roll angle; 0° , $+10^\circ$, $+20^\circ$, $+30^\circ$. The total broadside sector RCS is then characterized by seven roll angles and an average over a ten degree azimuth sector for seven azimuth angles at each roll angle. These forty-nine values are further divided into the upper sector (0° to $+30^\circ$) and lower sector (0° to -30°) consisting of twenty-eight values each (0° roll being common to each sector). Comparison between configurations is made based upon the arithmetic average of the ten degree average RCS values over the upper, lower and entire sector. These averages are determined by adding the twenty eight or forty-nine RCS values (depending on the sector) in square meters and dividing by the appropriate value. These averages are then converted to decibels relative to one square meter (dbsm) for presentation. Similarly the ten degree average RCS at each azimuth angle is plotted for each roll angle in dbsm as shown in Figure 2-2 for the triangular fuselage with a bottom-mounted supersonic wing. This data is at a frequency of 12 GHz. The sector average RCS values are also shown. The upper sector average RCS at 2, 4 and 12 GHz is shown in Table 2-1 for the four fuselage shapes, three wing locations and two sweep angles. Similar data for the lower sector and the entire sector are shown in Tables 2-2 and 2-3 respectively.

(U) The RCS calculations were checked against the measured RCS from a model of the circular body center subsonic wing configuration. The model also had a conventional T-tail. The agreement between measured and computed RCS for this model is, in general, good. There are observable discrepancies at some aspect angles which are attributed to traveling wave reflection. A subsequent investigation of traveling waves served to substantiate this conclusion. The computed RCS averaged over the broadside sector agrees with the measured data within 2.5 decibels.

(U) The influence of the empennage geometry on the broadside RCS was established for single tail, V-tail and twin tail configurations. The sector average RCS for each of these are shown in Table 2.4 for the top, bottom and entire broadside sector. These averages are obtained by averaging the RCS in square meters and then converting the average in decibels relative to one square meter (dbsm). This process is used throughout this report.

UNCLASSIFIED

D180-17939-1

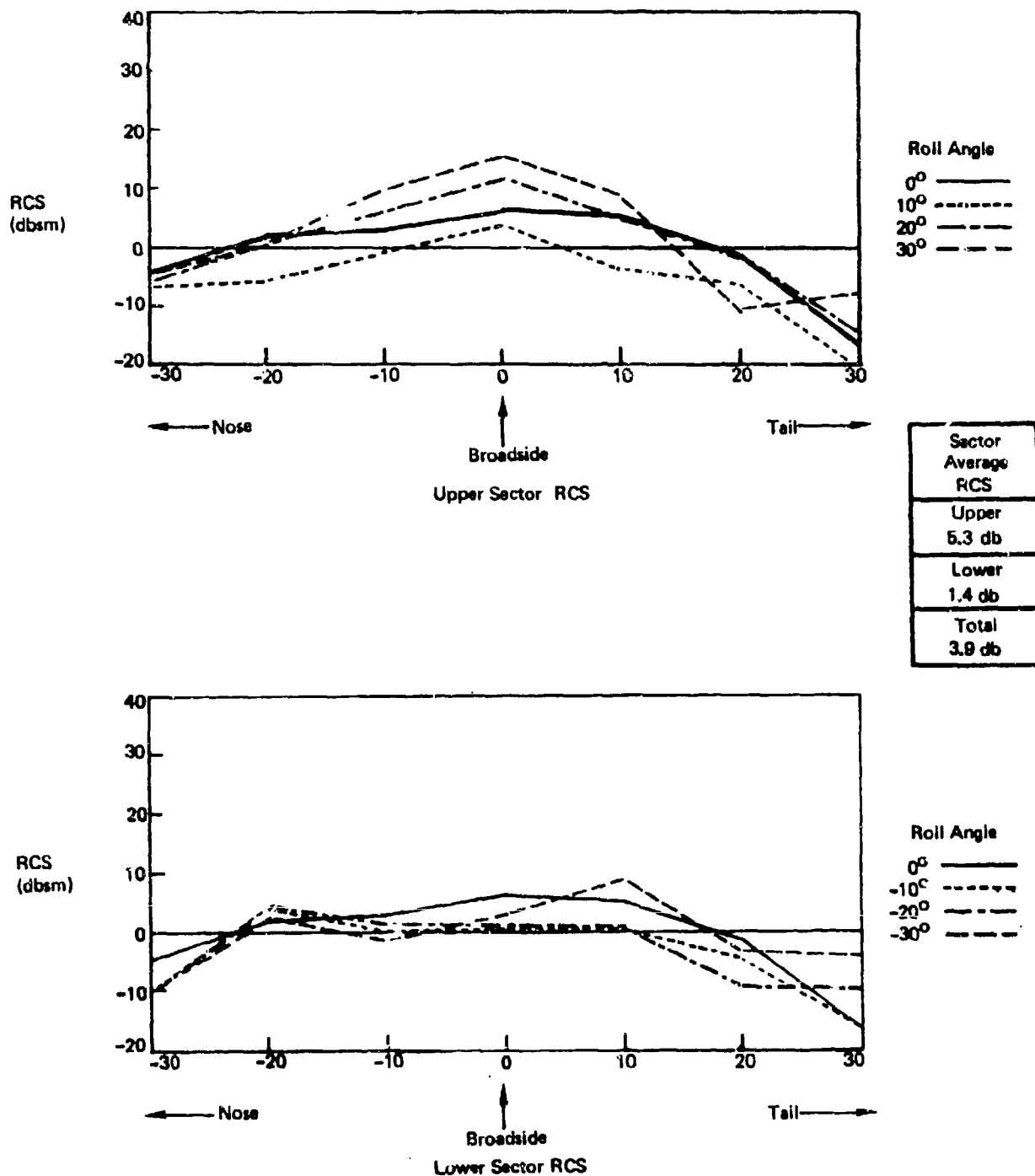


Figure 2-2: Computed RCS - Triangular Body - Bottom Supersonic Wing - 12 GHz (U)

UNCLASSIFIED
D180-17939-1

AVERAGE RCS (dbsm), 0° → + 30° ROLL, +30° YAW													
FUSELAGE SHAPE	WING SWEEP ↓	WING LOCATION											
		BOTTOM				CENTER				TOP			
		FREQUENCY				FREQUENCY				FREQUENCY			
		2 GHz	4 GHz	12 GHz	2 GHz	4 GHz	12 GHz	2 GHz	4 GHz	12 GHz	2 GHz	4 GHz	12 GHz
CIRCULAR	Sub- Sonic	17.7	17.9	16.8	13.5	11.8	10.8	14.6	10.7	6.9			
	Super Sonic	17.4	15.1	16.0	21.5	22.9	24.8	-	-	-			
	Sub- Sonic	17.1	13.6	11.7	14.6	13.6	6.9	-	-	-			
ELLIPT- ICAL	Super Sonic	15.8	13.2	8.4	27.7	27.6	27.1	-	-	-			
	Sub- Sonic	14.3	11.2	5.3	13.6	10.5	5.7	13.3	10.4	5.5			
	Super Sonic	14.5	12.0	5.3	14.7	14.5	21.5	15.2	13.1	7.8			
SQUARE	Sub- Sonic	21.6	24.2	26.3	17.1	18.7	21.4	-	-	-			
	Super Sonic	17.9	15.7	17.7	20.5	18.6	20.8	-	-	-			

RCS - UPPER BROADSIDE SECTOR (U)

TABLE 2.1

UNCLASSIFIED

UNCLASSIFIED

D180-17939-1

AVERAGE RCS (dbsm), 0° → + 30° ROLL, +30° YAW												
FUSELAGE SHAPE	WING SWEEP ↓	WING LOCATION										
		BOTTOM			CENTER			TOP				
		FREQUENCY			FREQUENCY			FREQUENCY				
		2 GHz	4 GHz	12 GHz	2 GHz	4 GHz	12 GHz	2 GHz	4 GHz	12 GHz	2 GHz	12 GHz
CIRCULAR	Sub-Sonic	9.1	7.3	4.1	9.8	7.4	5.2	14.9	16.6	17.3		
	Super-Sonic	9.1	6.8	5.6	10.3	8.3	5.6	-	-	-	-	-
	Sub-Sonic	8.0	5.0	2.8	9.3	8.0	7.4	-	-	-	-	-
ELLIPTICAL	Super-Sonic	7.9	4.2	3.3	9.4	7.4	7.0	-	-	-	-	-
	Sub-Sonic	7.8	3.2	0.1	9.4	6.5	4.6	8.6	4.9	2.0		
	Super-Sonic	8.4	4.7	1.4	9.5	7.2	8.1	9.8	7.1	6.7		
SQUARE	Sub-Sonic	14.8	13.2	8.9	18.7	19.8	20.9	-	-	-	-	-
	Super-Sonic	13.3	10.8	9.7	19.5	18.1	21.3					

RCS - LOWER BROADSIDE SECTOR (U)

TABLE 2.2

UNCLASSIFIED

UNCLASSIFIED

D180-17939-1

AVERAGE RCS (d.b.), 0° → + 30° ROLL, +30° YAW													
FUSELAGE SHAPE	WING SWEEP ↓	WING LOCATION											
		BOTTOM			CENTER			TOP					
		FREQUENCY			FREQUENCY			FREQUENCY					
		2 GHz	4 GHz	12 GHz	2 GHz	4 GHz	12 GHz	2 GHz	4 GHz	12 GHz	2 GHz	4 GHz	12 GHz
CIRCULAR	Sub-Sonic	15.6	15.7	14.5	11.9	10.4	9.2	15.0	15.1	15.1			
	Super-Sonic	15.3	13.0	13.8	19.3	20.6	22.5	-	-	-			
	Sub-Sonic	14.9	11.5	9.6	12.8	12.1	7.5						
ELLIPTICAL	Super-Sonic	13.6	11.1	6.5	25.3	25.2	24.7	-	-	-			
	Sub-Sonic	12.1	9.0	3.7	11.9	9.1	5.5	11.4	8.6	4.2			
	Super-Sonic	12.4	9.9	3.9	12.8	12.6	19.3	13.2	11.2	6.8			
TRI-ANGULAR	Sub-Sonic	19.5	21.9	23.9	17.9	19.6	21.7	-	-	-			
	Super-Sonic	15.8	13.6	15.7	19.4	19.1	21.6	-	-	-			
	Sub-Sonic												

RCS - ENTIRE BROADSIDE SECTOR (U)

TABLE 2.3

UNCLASSIFIED

D180-17939-1

EMPENNAGE	ENTIRE SECTOR			TOP SECTOR			BOTTOM SECTOR		
	+30° ROLL, +30° YAW			0° To +30° ROLL, +30° YAW			0° To -30° ROLL, +30° YAW		
	FREQUENCY			FREQUENCY			FREQUENCY		
	2 GHz	4 GHz	12 GHz	2 GHz	4 GHz	12 GHz	2 GHz	4 GHz	12 GHz
SINGLE TAIL	11.9	10.4	9.2	13.5	11.8	10.8	9.8	7.4	5.2
V-TAIL	8.2	7.4	4.8	7.4	6.8	5.5	8.5	7.6	3.1
TWIN TAIL	9.7	8.0	6.7	8.2	8.1	6.9	8.4	7.1	5.7

All values are average of RCS (dbsm) over the particular sector.

All values are for a centered subsonic wing and a circular body.

Table 2.4 EMPENNAGE COMPARISON (U)

~~SECRET~~

D180-17939-1

(C) During the preceding study under this contract, an expression for calculating the traveling wave reflections from flat rectangular plates, was developed. This current program has expanded on that work and has examined plates terminated with right angle and cylindrical surfaces of various sizes. This work was motivated by the observable discrepancies between RCS data measured from a model and that calculated from a computer program which can predict geometric optics returns but not traveling wave returns. In addition to plate terminations, the influence of plate curvature on traveling waves was also examined. The results of the plate studies show that the RCS due to traveling wave reflection can, at specific viewing angles, approach hundreds of square meters. The average RCS over the entire broadside sector will be much lower (near one square meter) for the traveling wave reflections but they can still be significant to a low RCS design.

(S) The specular and traveling wave RCS contributions were used as design guidelines to select the configuration of the aircraft shown in Figure 4.1. This is a photograph of a model of the "Low RCS Airplane" conceived during a previous Navy program at Boeing. The RCS of this configuration was originally estimated to be 10 square meters averaged over the lower (0° to -30° roll) broadside sector. This original estimate was based upon a very simplified analysis. The design guideline data developed during this latest program has shown that the average RCS of the airplane should be below the 10 square meters originally estimated. This conclusion is verified from RCS measurements on the model shown in the Figure. The RCS of this model was measured at a frequency corresponding to 4 GHz. The ten degree median RCS of this airplane does not exceed 10 square meters at any point in the lower (0° to -30° roll) broadside sector. The average of the ten degree median RCS over this sector is near 2.0 square meters. This RCS is about a factor of ten lower than for a conventional aircraft. This indicates a sufficient degree of RCS control to enable use of active ECM systems to protect against radar guided threats. This makes possible a degree of survivability which is not possible for conventional aircraft within today's technology. This improvement in RCS is at minimal cost and with no significant performance decrease.

~~SECRET~~

~~CONFIDENTIAL~~

D180-17939-1

(Additional RCS reduction can be realized by applying absorber treatments. However, in order to achieve another factor of ten reduction in the broadside RCS an extensive absorber treatment is required. The markedly low level of RCS achieved in the broadside sector indicated that this degree of treatment is not warranted for this particular airplane. However, other aircraft may very well require additional RCS control and extensive absorber may be readily justified.

~~(C)~~ The results of this study have shown that substantial broadside RCS control is attainable by careful control of the airplane configuration. The results also indicate the existence of sufficient traveling wave reflections to warrant concern at low levels of RCS. Control of these reflections is readily achieved by appropriately shaping and terminating planar surfaces. In general, the control of aircraft RCS in the broadside sector is shown to be feasible and practical.

~~CONFIDENTIAL~~

UNCLASSIFIED

D180-17939-1

3.0 Technical Approach (U)

(U) A supersonic fighter aircraft configuration developed during the Boeing participation in the Navy HIPAAS Program, was chosen as the baseline airplane for this study. A series of configurations having the same volume, wing and tail area as the baseline, were modeled on the computer. The RCS was calculated at each point of the broadside sector for each of the various configurations of fuselage shape, wing shape and location and empennage geometry. The computer calculations were verified by experimental analysis on a scale model of one configuration. An analysis was also made to determine the influence of traveling waves on the RCS in the broadside sector.

(U) The design guideline data obtained for the various configurations was used, along with guidance from structures, aerodynamics and propulsion personnel, to configure a "Low RCS Aircraft".

3.1 Methodology (U)

(U) The supersonic fighter aircraft proposed by Boeing on the Navy HIPAAS project is shown in Figure 3.1. It is 60 feet long with a subsonic wing span of 45 feet. In order to develop the various configurations for this study, the engine inlets and canopy were removed from this aircraft and drawings then made at each section so that the area was preserved but the shape modified. Thus, the volume of the aircraft was not changed but the outer surface of the aircraft modified to reflect the various fuselage shapes under study. The 1/8th scale model shown in Figure 3.2 was built from the circular fuselage drawings so produced. The same drawings were used to define the aircraft for the computer calculation of the RCS.

(U) The RCS of the model was measured at 33 GHz on the 1000 feet outdoor RCS range, to obtain 10° medianized RCS values over the broadside sector. The measured medianized RCS values were compared to the computer calculated values to verify the utility of the computer program for determining the RCS of this and the other configurations under study.

UNCLASSIFIED

DI80-17939-1

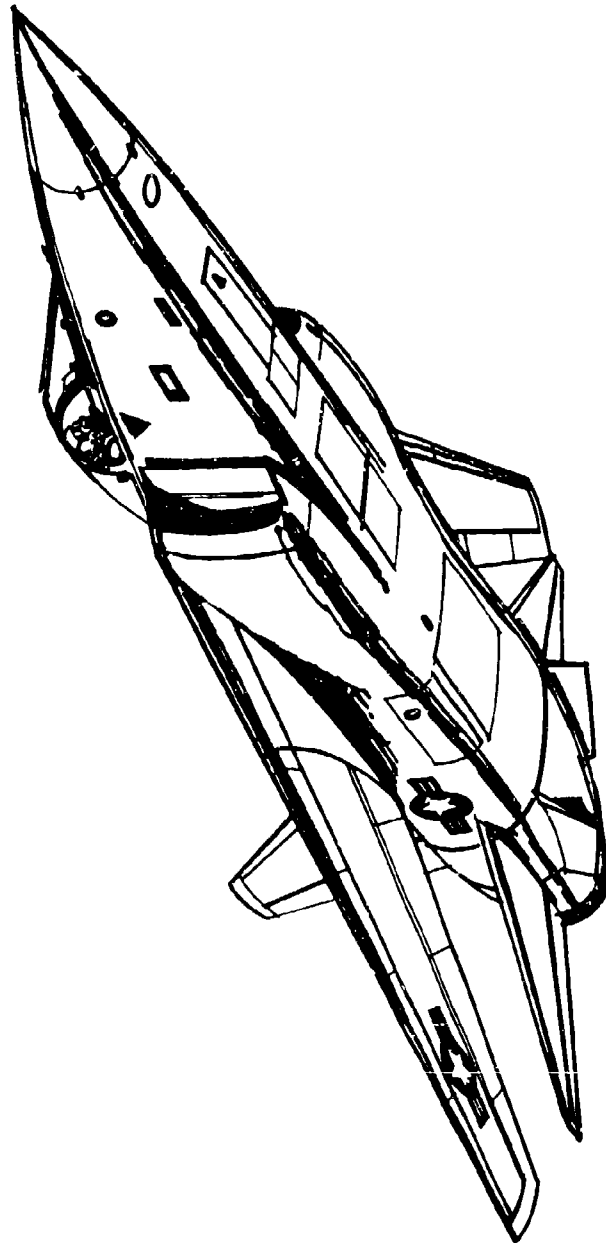


Figure 3-1: Supersonic HIPAAS Airplane (U)



Figure 3-2: Circular Fuselage Model (U)

UNCLASSIFIED

D180-17939-1

3.1.1 Aircraft Definition (U)

(U)Nine body sections were taken from the HIPAAS aircraft drawings. The canopy and inlets were removed and the area of each section then determined by a planimeter. The section area was kept constant for each of the different fuselage shapes subsequently developed, circular, square, triangular and elliptical. In addition, sharp corners were not allowed on the triangular and square bodies. The corners were rounded with a minimum (full scale) radius of curvature of 5 inches. The area of each sector was maintained constant to compensate for the rounded corners. The tail was included with no changes from the HIPAAS drawings. The variable sweep wings were converted to two separate wings - one supersonic and one completely subsonic. The wings maintained the basic airfoil shape, but were made symmetrical top to bottom. This was for ease of definition of the computer model. The circular fuselage configuration was constructed to one-eighth scale of the computer model and the RCS determined by measurement and computation respectively.

3.1.2 Computer Analysis (U)

(U)The various airplane configurations were described as a series of curves and stringers for computer input. Each airplane was segmented into components: fuselage, wing, horizontal stabilizer and vertical stabilizers. The wing, for instance, is described by 10 curves and 17 stringers. Each curve is made up of 17 points. The line joining the same point on each curve is a stringer. These are shown in Figure 3-3.

(U)At intersection points of the curves and stringers, the tangents (both along the curves and along the stringers) are determined by the parallel chord method.

(U)A parallel grid of specimen rays are then "thrown" at the body. This determines which curves and stringers of which components are visible for each direction of the incident energy. From this definition of the visible surface, a much larger number of rays ($10^5 - 10^6$) are directed toward the visible surface. Each ray is traced using the rule: angle of incidence equals angle of reflection, up to and including double reflections. The normal at each point of the surface where the ray strikes, is determined by warped surface interpolation.

UNCLASSIFIED

D180-17939-1

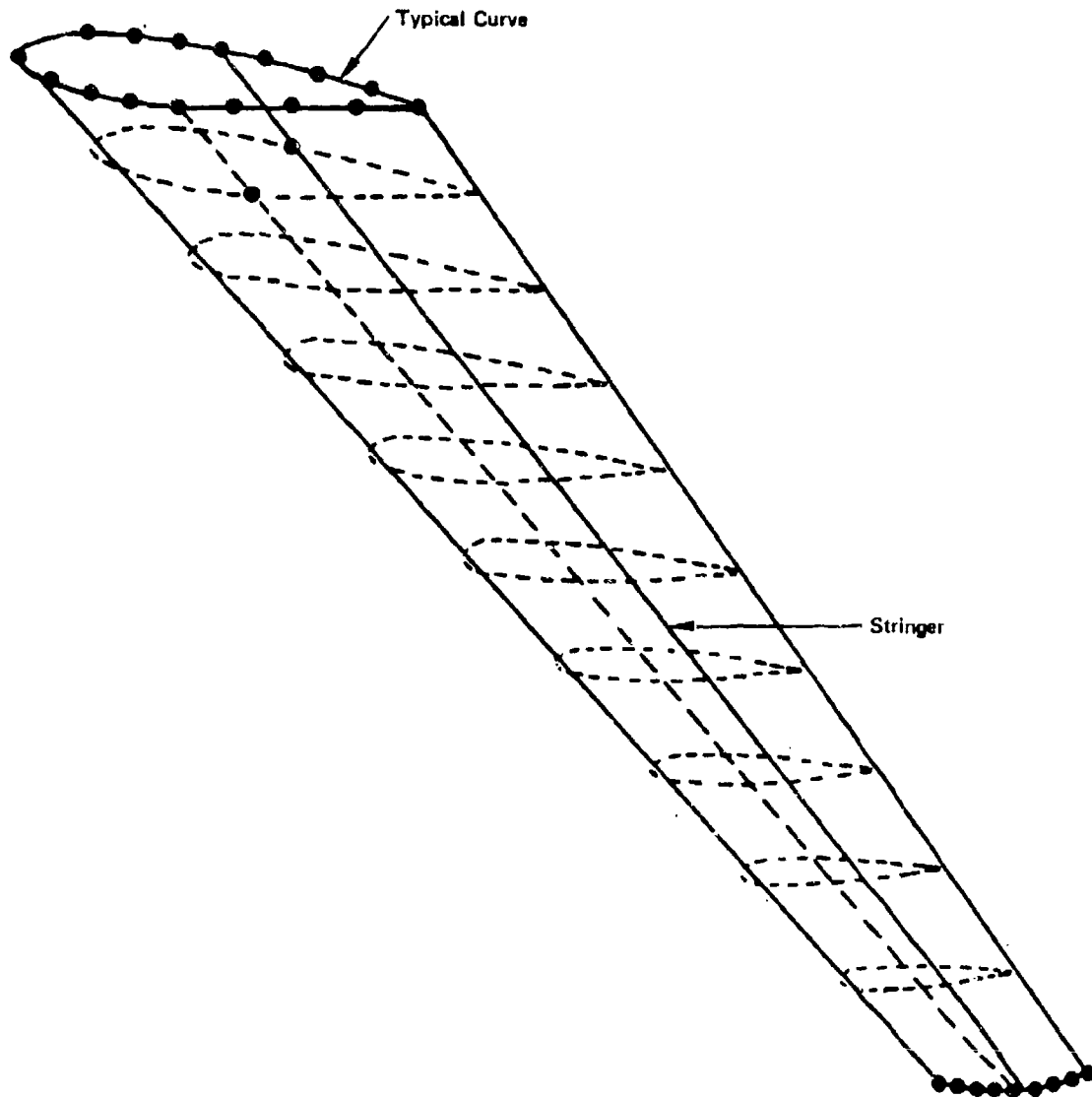


Figure 3-3: Definition of Wing to the Computer (U)

UNCLASSIFIED

D180-17939-1

(U) A radiation sphere is then centered on the body. It is divided into 1,252 elements of surface area, each measuring approximately 33 square degrees. Each reflected ray is traced to determine which element (angular box) of the radiation sphere through which the ray passes. The relative phase of a particular ray is determined by comparing the path length of that ray with the path length of the "reference ray". The reference ray is reflected from an infinitesimal sphere located at the origin of coordinates in the direction of the given ray.

(U) Each ray is treated as a Poynting vector and is considered to carry a unit of power. Since the energy is coherent and polarized, phase and polarization must be respected in the summation of the reflected rays to yield the energy of a given polarization reflected in a given direction. The magnitude of the phase sum in each of two orthogonal polarizations is proportional to the scattering cross section for that polarization at the nominal angle of the angular box. This gives the RCS for a particular incident angle.

(U) This procedure was repeated at each of the angles of interest in the broadside sector for each of the different airplane configurations under consideration. Thus, the RCS was determined at 49 points ($+30^\circ$ in azimuth by $+30^\circ$ in elevation in 10° intervals) of the broadside sector for each configuration. Four fuselage shapes, circular, triangular, square and elliptical, were compared for the different wing locations - bottom, center and top, and two wing shapes - supersonic and subsonic. Also included in the configuration studies were various empennage geometries including the normal T-tail, V-tail, and twin tail shown in Figure 3.4. These were compared only for the circular fuselage shape and a centered subsonic wing. The results are tabulated in Section 2 and discussed in Section 3.2.

3.1.3. Wing/Empennage Fairings (U)

(U) The circular fuselage model shown in Figure 3.2 was made in the Boeing model shop. The right side of the model had metallic fairings inserted at the wing and tail joints to the fuselage. Azimuth patterns for seven different roll angles (from -30° roll to $+30^\circ$ roll) were taken. The effect of the fairings on the broadside sector ten degree median RCS is shown in the following two figures. Figure 3-5 shows the ten degree median RCS for each of the roll angles for vertical polarization without fairings. Figure 3-6 is the RCS values for the same roll angles and polarization for the same circular body airplane with fairings - both at ± 33 GHz. The fairing effects are most noticeable

D180-17939-1
UNCLASSIFIED

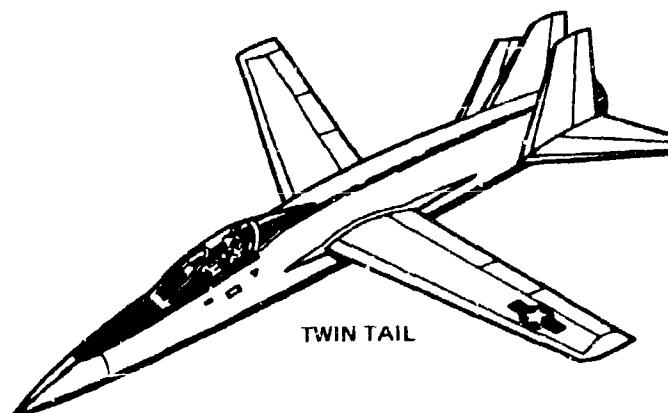
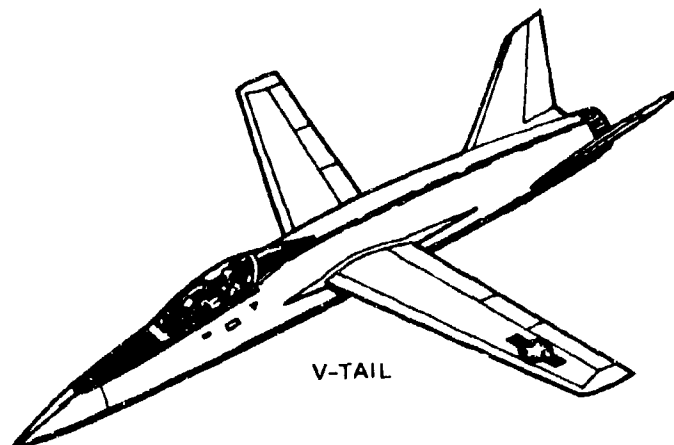
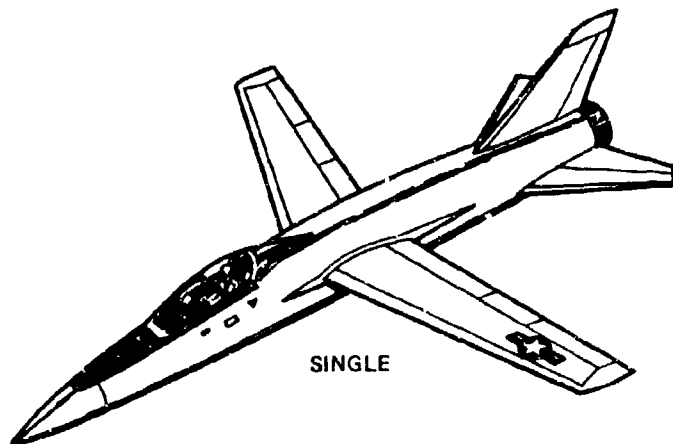


Figure 3-4: Empennage Geometry (U)

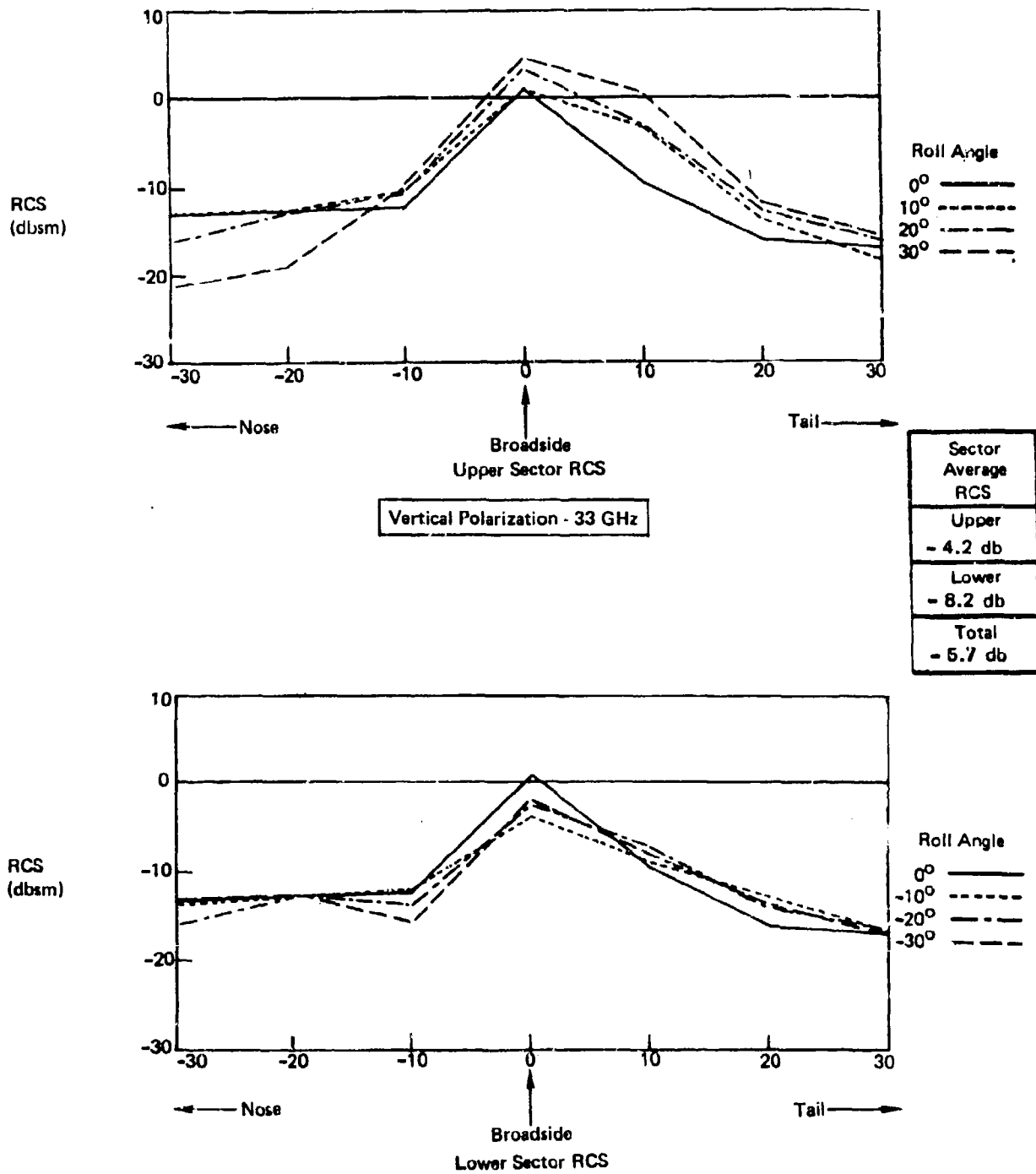


Figure 3.5: Measured RCS - Circular Model (U)

UNCLASSIFIED

D180-17939-1

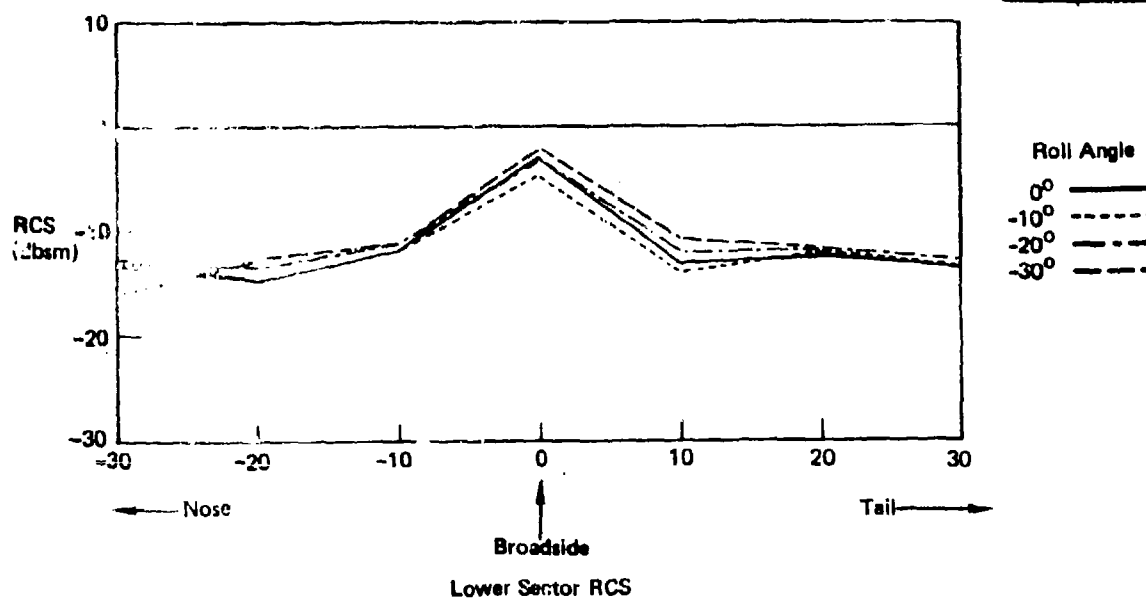
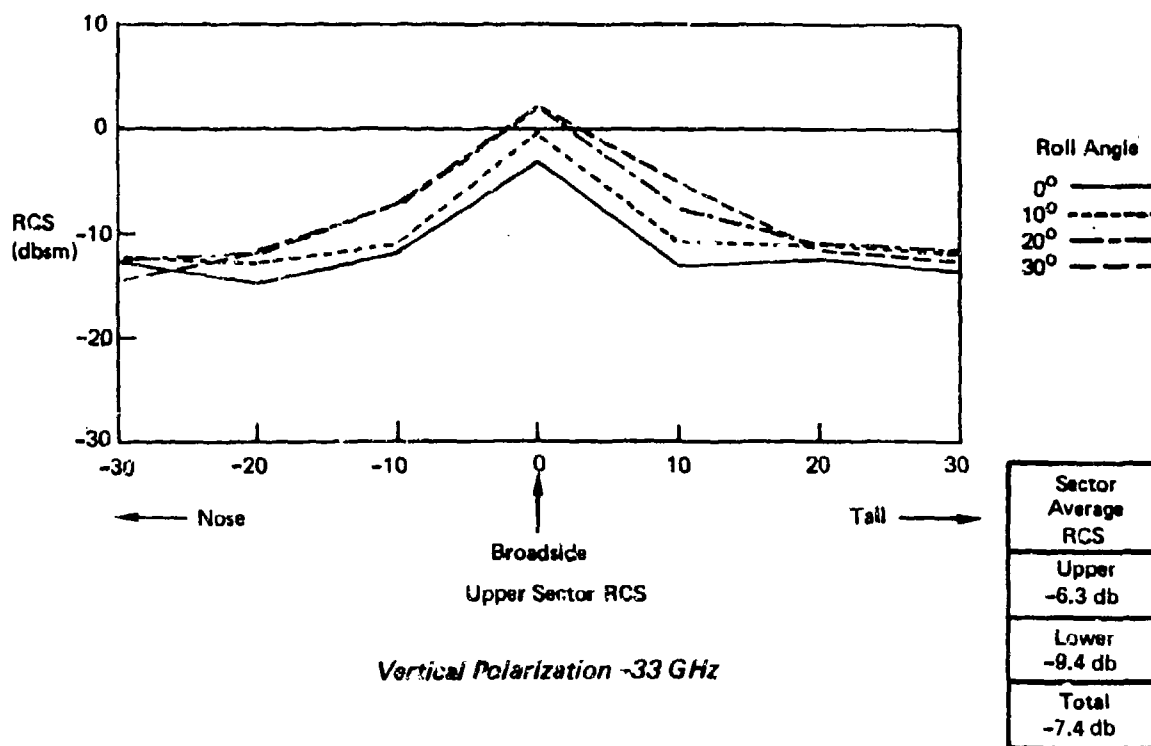


Figure 3.6: Measured RCS - Circular Model With Fairings (U)

UNCLASSIFIED

D180-17939-1

(U)

at vertical polarization due to the presence of traveling waves at this polarization. These waves are discussed in Section 3.1.5. The fairings show a reduction in RCS over the majority of the broadside sector.

3.1.4 Computer Model Verification (U)

(U)The RCS of the circular body model was measured as discussed above at 33 GHz for the seven different roll angles. The 10° median values in the broadside sector were determined and compared with the computer calculated RCS values for both horizontal and vertical polarizations. The RCS for the individual roll angles is shown in Figures 3-7 for the computed values, Figure 3-8 for the vertical polarized measured values and Figure 3-9 for the horizontally polarized measured values.

(U)When the range measurements were taken, it was only possible to obtain a -25 dbsm tower plus background level due to the weather. Thus, it was not possible to obtain accurate median RCS values lower than about -20 db. This accounts for the large differences at the extreme angles fore and aft of the sector where the computed values are quite low.

(U)Generally, the agreement is very good for values of RCS higher than the measurement background. For the measured vertical polarization results, the values at $+10^{\circ}$ in azimuth about the left broadside, are higher due to the traveling wave discussed below. The agreement obtained between the geometric optics RCS computer program and the range measured RCS values demonstrates that the trend data obtained by the program for the various fuselage shapes and wing shapes and locations, accurately reflects the differences in aircraft RCS due to the configuration.

UNCLASSIFIED

D180-17939-1

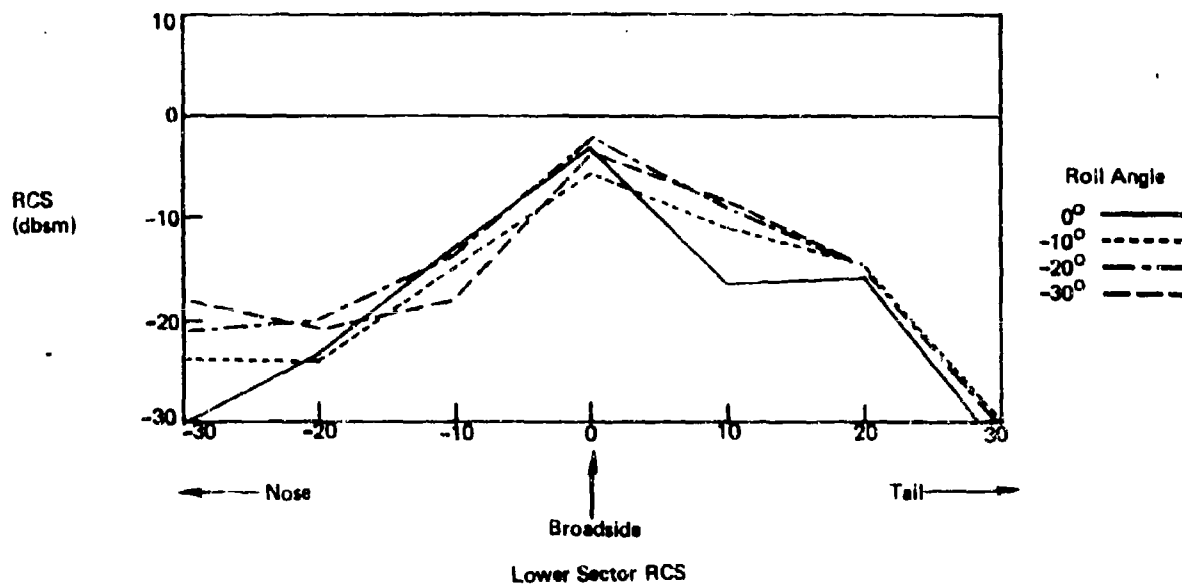
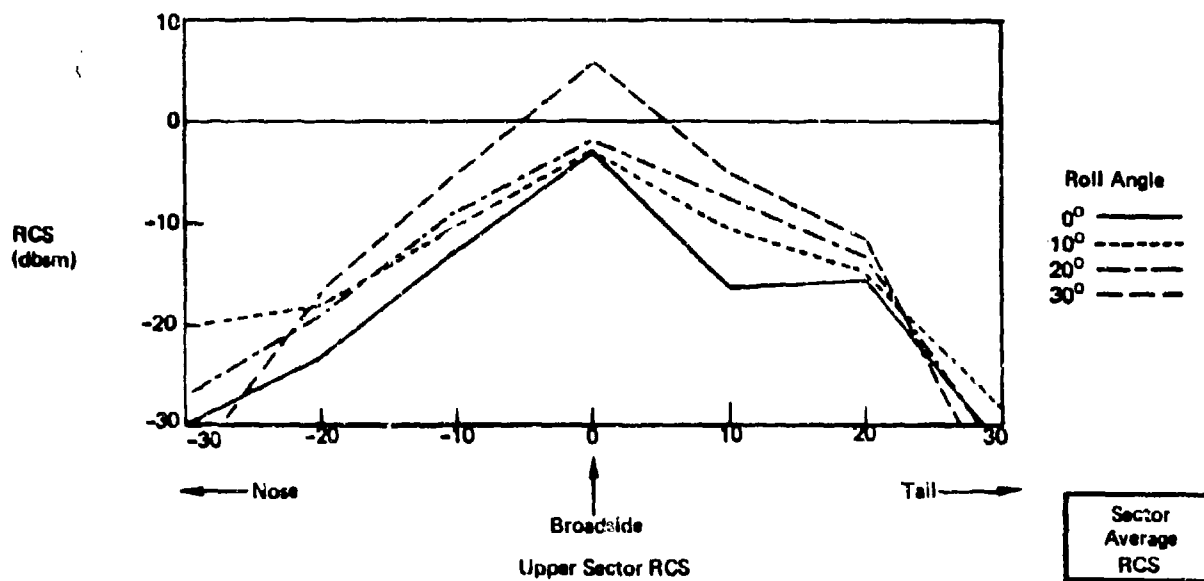


Figure 3.7: Computed RCS Circular Model - 32 GHz (U)

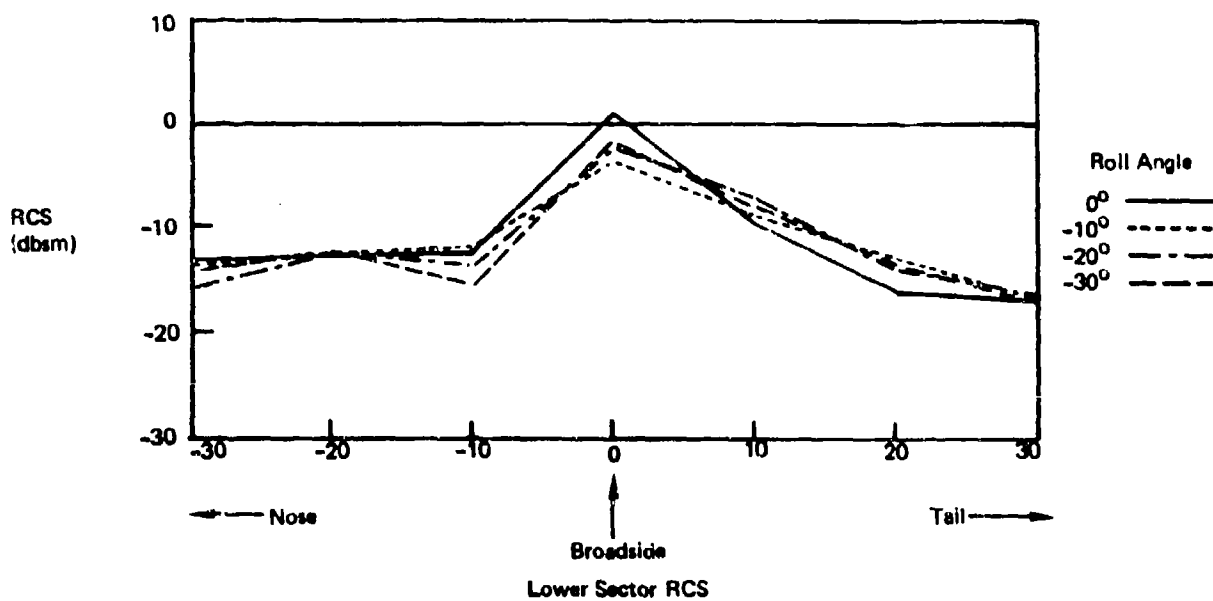
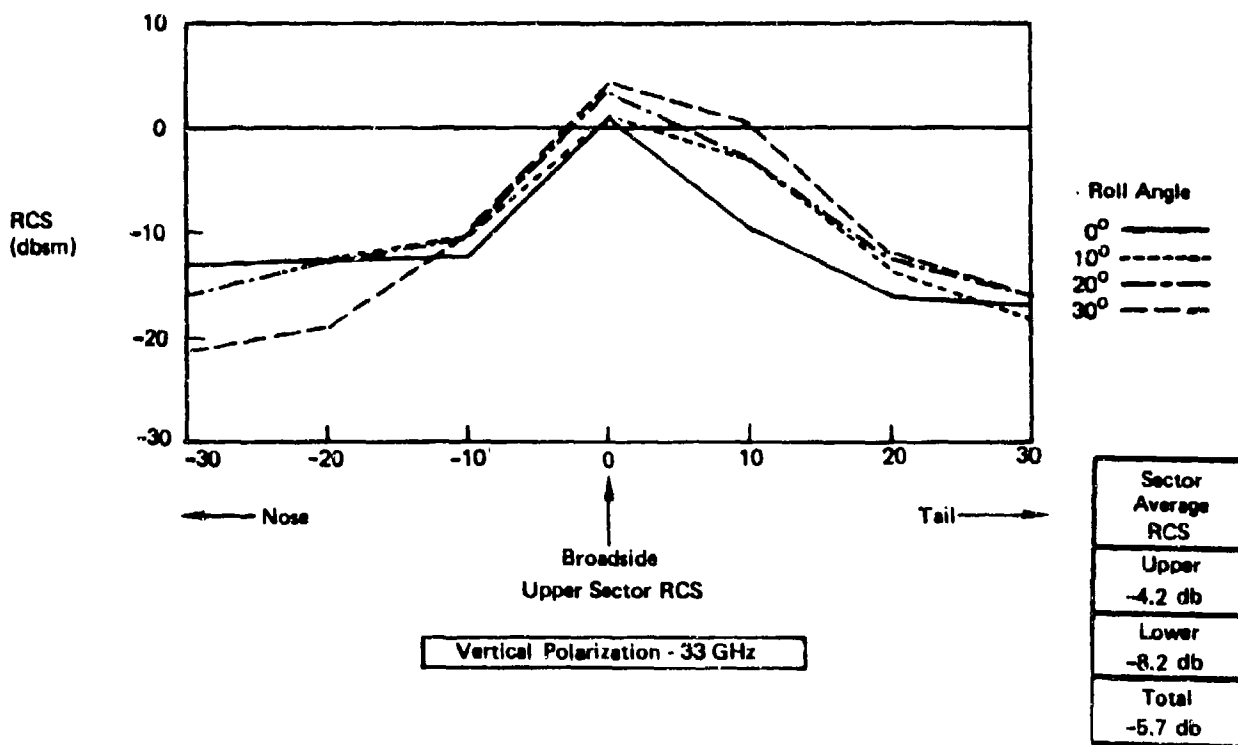


Figure 3.8 : Measured RCS - Circular Model (U)

UNCLASSIFIED

D180-17939-1

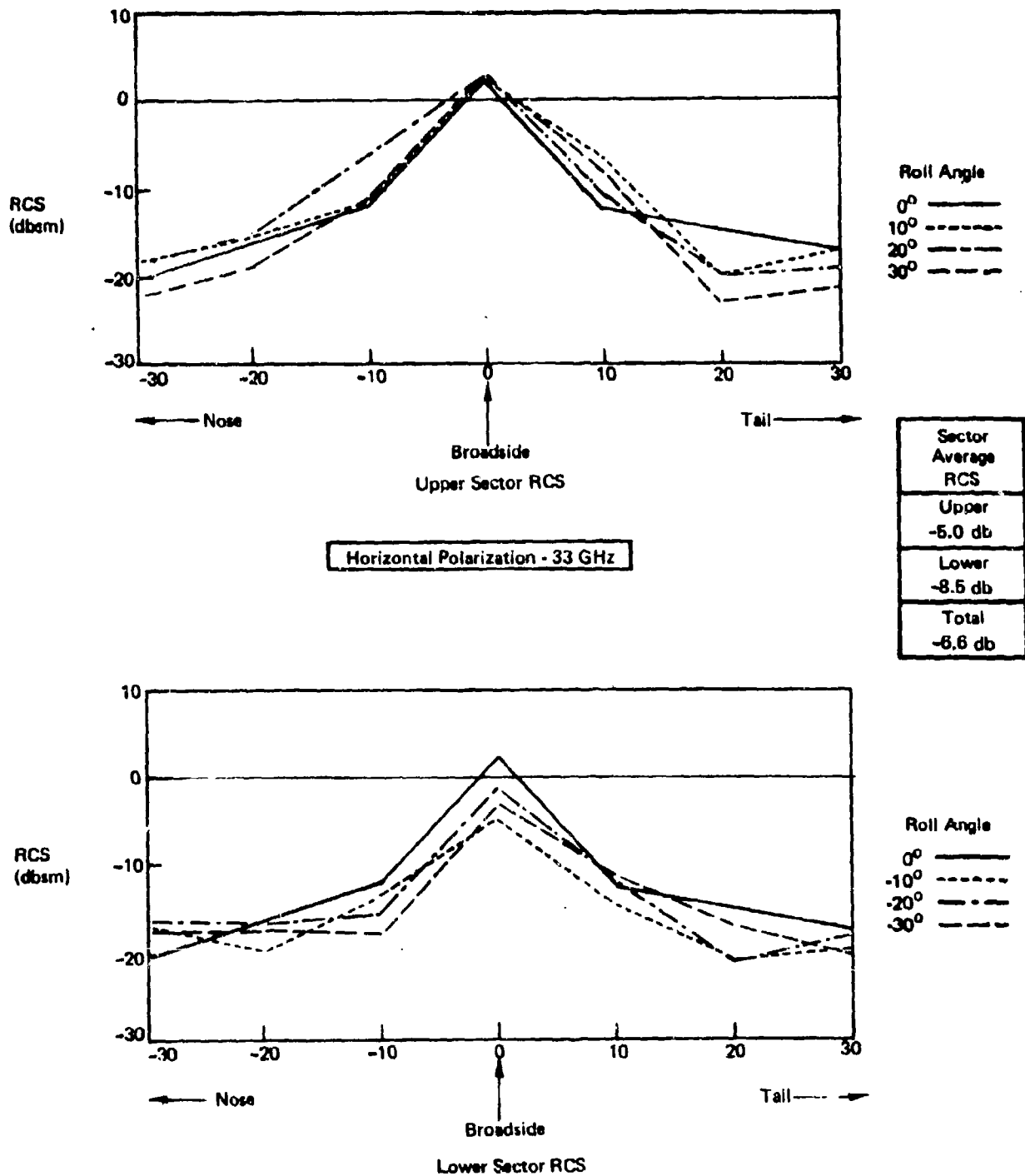


Figure 3.9 : Measured RCS - Circular Model Measurements (U)

UNCLASSIFIED

D180-17939-1

3.1.5 Traveling Waves (U)

(U) The various experimental tests conducted during this program have clearly established the presence of RCS contributions from other than specular or quasi-optical electromagnetic reflections. These RCS contributions occur at near grazing incidence for electric fields oriented normal to a planar surface. These are attributed to reflections of "traveling waves" by discontinuities along a plane surface. The terms "traveling wave" and "surface wave" are frequently used to describe electromagnetic waves propagating along a boundary between two media.

(U) "Surface wave" is a class of waves propagating along a general surface with a propagation constant comprised of an attenuation factor, α and phase factor β . The propagation of a surface wave will depend on the surface characteristics. The surface impedance ($Z_s = R_s + jX_s$) is frequently used to describe a surface and in turn the propagating characteristics of the various surface waves which can propagate along a plane surface. A metal surface of infinite conductivity will have a surface impedance $Z_s = 0$. However, the large finite conductivity of actual metals will result in a surface impedance $R_s + jX_s$ where R_s and X_s are slightly greater than zero. This special case of a surface wave along a surface of high conductivity could correspond to a traveling wave along a metal surface.

(U) There is no well-established consensus as to the definition of a traveling wave as opposed to a surface wave. A wave traveling along a metal surface does not behave as a surface wave along an impedance boundary. The rate of decay of the fields away from the surface appears to be more rapid for a metal surface than would be expected based on surface wave theory.

(U) To clarify the following discussions the terms as used in this report are defined as:

- (U) Traveling waves are electromagnetic waves propagating along a high-conductivity relatively flat metal surface.
- (U) Surface waves are defined as propagating along a general impedance boundary and may or may not include traveling waves as a special case.

UNCLASSIFIED

D180-17939-1

(U) The definition of these two types of electromagnetic waves is germane to the subject of aircraft RCS as both types can constitute major sources of RCS. Traveling waves (as defined) can exist along the flat metal surfaces of an aircraft and upon reflection (and radiation) can provide substantial RCS levels. Surface waves can exist along (or within) various dielectric surfaces (radomes, absorbers, windows) as well as along non-planar metal surfaces. These surface waves also contribute to the aircraft RCS upon reflection and radiation.

(U) The traveling waves are considered the more predominant RCS contributor of the two wave types due to the large amount of metal surfaces present on most aircraft. However, in the case of the AGM-69-A (SRAM) missile a dielectric heat shield was applied over the missile body and a substantial surface wave was supported. This wave was a major contributor to the SRAM radar cross section. The control of the SRAM RCS to the extremely low levels attained, required that the surface wave reflections be carefully controlled.

(U) The significance of traveling waves to airplane RCS is determined by the level of RCS desired. The earlier studies conducted under this present contract show that traveling wave reflections can be significant for aircraft designed to have an RCS below 1 square meter in the forward and aft sectors. However, it was felt that the traveling wave RCS contribution in the broadside sector would be of lesser significance due to the large specular reflections normally present. The results of this present study indicate that the traveling wave RCS contribution is, in fact, much more substantial than previously expected, especially in the broadside sector.

(U) During the preceding study, the following expression was developed to calculate the traveling RCS from a flat plane surface:

$$\sigma = 10 W \lambda \gamma F(\theta) G(\phi)$$

Where

$$F(\theta) = \cos^8[2(\theta + \theta_n)] \sin^2[(2\pi L/\lambda) \sin^2(\pi/4 - \theta/2)]$$

$$G(\phi) = [\cos \phi \sin(4\pi W/\lambda \sin \phi / ((4\pi W/\lambda) \sin \phi))]^2$$

And:

L = Plate length

W = Plate Width

θ_n = Position of lobe maxima from surface normal

γ = Reflection factor

λ = Wavelength

UNCLASSIFIED

D180-17939-1

(U)The $G(\phi)$ expression has been added to the previously reported formula and is based on the observed dependence of the traveling wave RCS in the ϕ plane. The coordinate system (θ, ϕ) , is shown in Figure 3-10 as are illustrations of some typical traveling wave reflections from flat plates.

(U)The preceding expressions are not intended to represent a rigorous analysis of the traveling wave phenomena but are a means for estimating the approximate level and spatial distribution of the RCS due to traveling wave reflections from edges of flat planar surfaces. The accuracy of the expression will not be addressed herein other than to note that good agreement has been observed between the RCS calculated using these expressions and measured RCS data on several flat rectangular plates.

(U)The term γ is a reflection factor which has been arbitrarily defined as a multiplying power factor determined by the termination geometry at the rear of the planar surface. A zero height abrupt edge is defined here to have a unity reflection factor.

(U)The previous studies under this contract have studied flat plates with a zero height ($\gamma = 1$) termination. The RCS from these plates due to traveling waves are, in general, below 1 square meter. However, the wing and empennage surfaces of an airplane have near planar surfaces which are terminated at the fuselage in other than an abrupt edge. Therefore, it was necessary to determine a relationship between the traveling wave reflection factor (γ) and the terminating geometry in order to estimate the traveling wave contribution to the RCS in the broadside sector.

(U)A series of one foot by two foot rectangular flat plate test models were built with right angle termination of 1/16, 1/8, 1/4, 1/2 and 1 inch height. The magnitude of the traveling wave reflection was then measured for each termination and the ratio (γ) to the reflection from a zero height termination was established. The results of these tests are shown in Figure 3-11. In addition, the γ for two cylindrical terminations with diameters of 5.3 and 12.5 wavelengths were measured and are also shown. The tests show that a γ of 100-200 is associated with an abrupt termination over 1.5 wavelengths high. This is clearly the case for the wing and tail surfaces which are terminated abruptly at the fuselage. This would be the case for most aircraft of conventional designs.

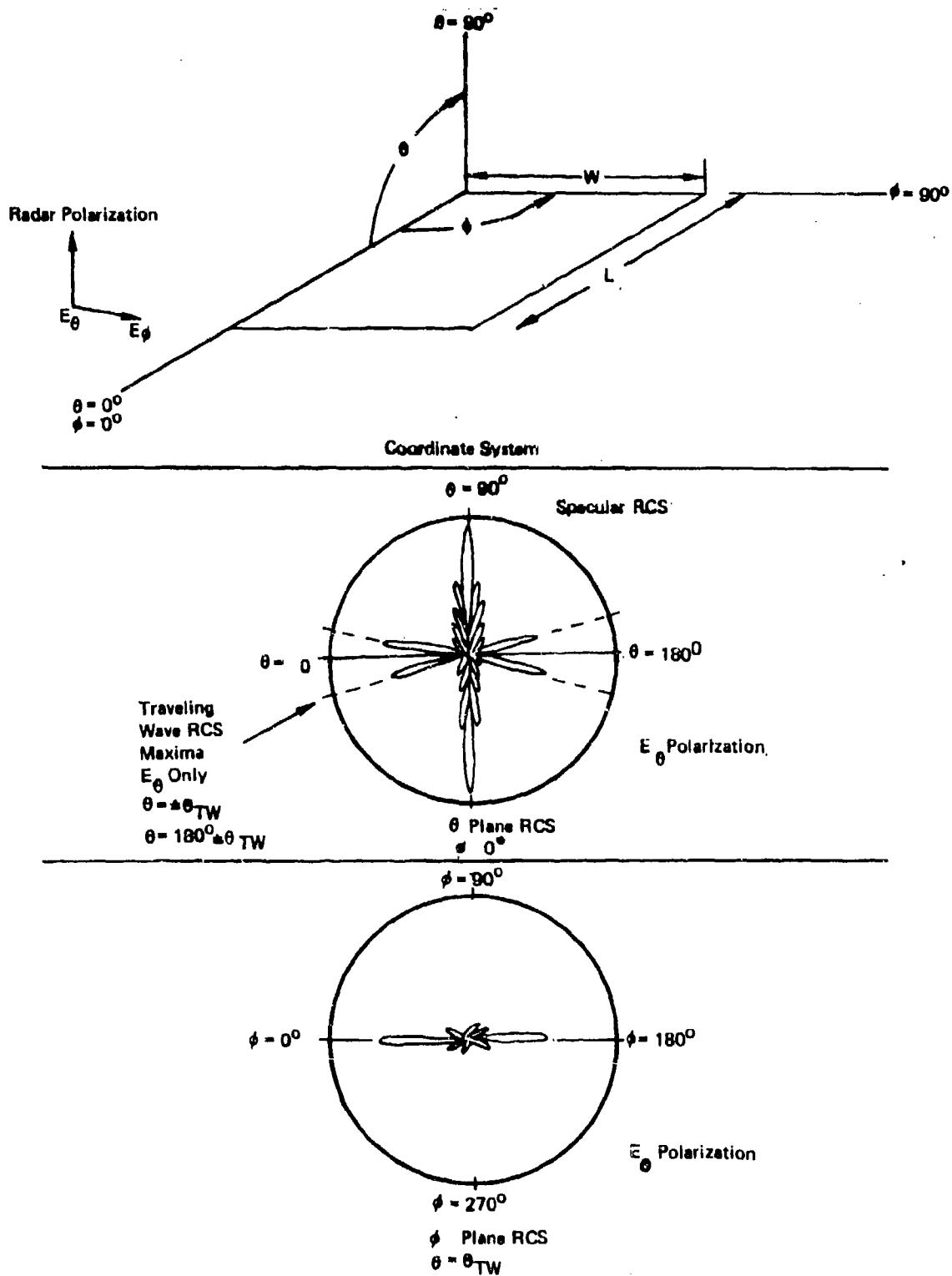


Figure 3.10: Flat Plate RCS (U)

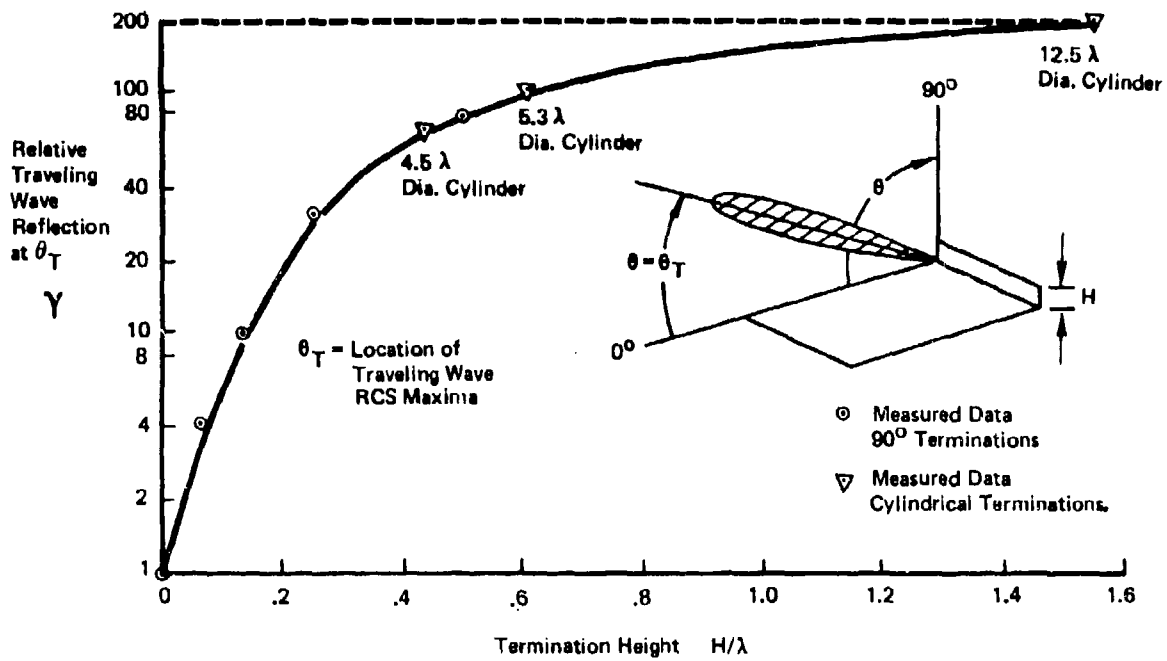


Figure 3.11: Traveling Wave Reflection Coefficient $\gamma(U)$

UNCLASSIFIED

D180-17939-1

(U) A reflection factor of 100-200 can result in traveling wave reflections which reach levels near 100 square meters for typical aircraft wing or tail surfaces. This large RCS is normally confined to a relatively narrow angular sector. Inasmuch as a radar will "view" a target over an angular sector on the order of 5 or 10 degrees, it is logical to use average values of RCS over similar angular sectors. Therefore, the traveling wave reflection was calculated over a ten degree solid angle for rectangular flat plates as a function of plate length and width. This average RCS is shown in Figure 3-12 for a γ of 100. The average traveling wave reflection is directly proportional to γ as defined. An average RCS due to traveling wave reflections near 10 square meters is representative for many regions on an aircraft. This level is not significant to the total RCS of typical aircraft where the average ten degree RCS will exceed 100 square meters. However, a 10 square meter RCS can be significant for an aircraft designed to have a low RCS (below ten square meters). Therefore, whenever possible flat surfaces should be terminated with electrically smooth transitions which have a low traveling wave reflection factor (γ).

(U) Traveling waves will propagate along a curved surface although energy is radiated continuously as the wave propagates. The amount of radiated energy is determined by the radius of curvature of the surface relative to the radar wavelength. A measure of the amount of radiation occurring for a traveling wave along a curved surface was obtained through a series of RCS measurements on curved plate models.

(U) This experiment was conducted by curving 1 foot by 3 foot rectangular plates along the 3 foot dimension. The peak traveling wave return reflected from the terminating edge of each plate was measured and compared to that from a flat plate. The traveling wave returns become difficult to identify as the radius of curvature of the plates decrease below 100 wavelengths. Therefore, the curvatures were restricted to values between 100 and 1000 wavelengths. The traveling wave returns were measured for three different right angle plate terminations of different heights. The resulting RCS for each plate is shown in Figure 3-13 as a function of radius of curvature of the surface. The curve drawn through the points is to show a general trend. More data is required to establish an exact dependence of the traveling waves on curvature. However, it is apparent from the data shown that a factor of ten reduction in traveling wave RCS is likely for surfaces having a radius of

UNCLASSIFIED
D180-17939-1

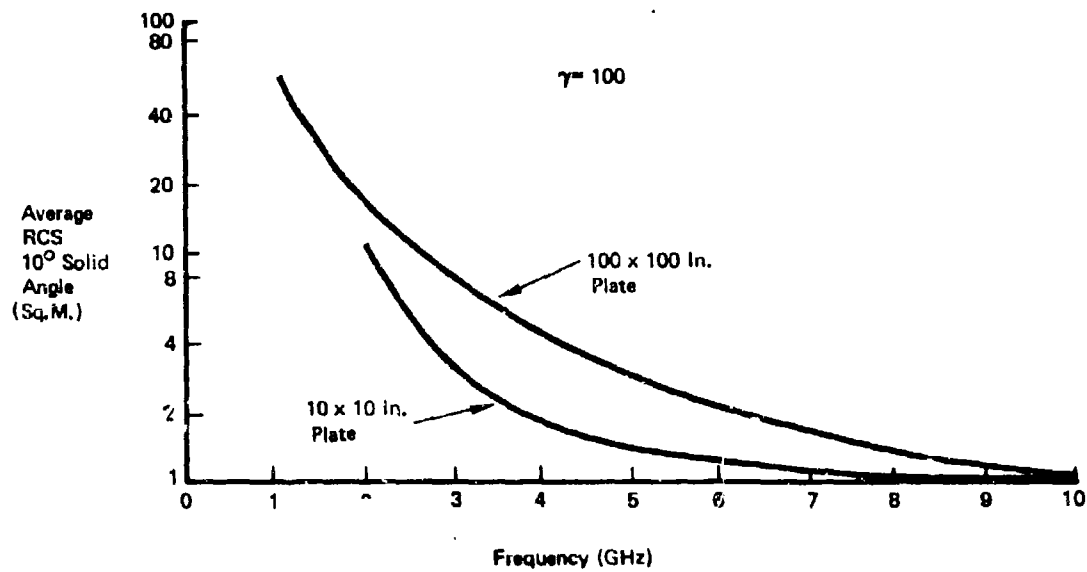


Figure 3.12: Traveling Wave RCS (U)

UNCLASSIFIED
D180-17939-1

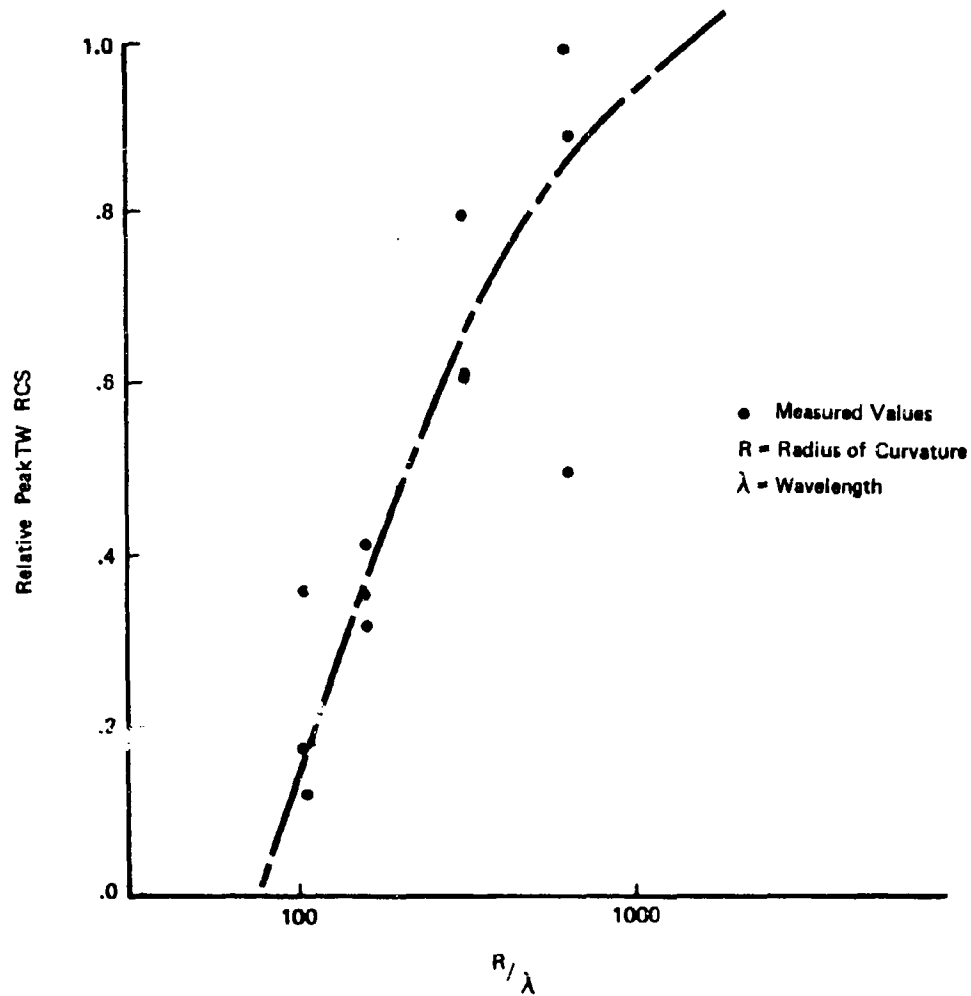


Figure 3.13: Traveling Wave Reflection vs Radius of Curvature (U)

UNCLASSIFIED

D180-17939-1

(U) curvature below 100 wavelengths. The RCS from aircraft due to traveling waves appears to be predominately from the flat surfaces.² This is apparently due to the rapid decay in the traveling waves with curvature as noted.

(U) The influence of traveling waves on broadside RCS can be seen by comparing Figures 3-7 and 3-8. The computed specular RCS of the circular fuselage airplane is shown in the plot of Figure 3-7 and the similar measured RCS is shown in Figure 3-8 for a vertically polarized radar. The planar surface of the horizontal stabilizer and wing should contribute a traveling wave return at aspects near ten degrees from broadside towards tail-on. A "peak" in the RCS for the measured RCS (Figure 3-8) appears near ten degrees from broadside sector. This "peak" is not predominate for either the computed specular RCS or for the measured RCS at horizontal polarization (traveling waves will not propagate along a horizontal surface for horizontal polarization). The values shown in the Figures are the model RCS at 33 GHz. The full scale airplane would be a factor of 64 (18 db) larger and the frequency would be 4 GHz. The "plateau" shown in the measured data for levels near -20 dbsm ($.01 M^2$) is due to the limiting "background" of the measurement system.

(U) The influence of the traveling waves on the broadside RCS can be minimized by fairing the various joins and terminations for the critical airframe surfaces. It is important that the presence of the traveling waves be kept in mind when considering RCS control. Failure to account for traveling wave reflections can result in unwarranted increases in the RCS levels.

3.1.6 Absorber Installations (U)

(U) The use of radar absorbing material (RAM) to control RCS in the broadside sector presents several unique problems. If RAM is the only means of RCS control employed (i.e., no shaping or configuration control) then a very high degree of absorption (20-30 db) is necessary to provide a sizable reduction in RCS. This in turn implies a fairly thick material for high absorption at lower micro-wave frequencies (1-4 GHz). The installation of absorbers as part of the airframe surface can create surface discontinuities between the edges of the RAM and adjacent structure. These surface discontinuities will constitute points of reflection for the electromagnetic waves propagating along the surface. These reflections can be substantial and of significance at low RCS levels (below 1 square meter). A preliminary study

UNCLASSIFIED

D180-17939-1

(U) into the RCS characteristics of absorber installations was made using the test fixture of Figure 3-14. This fixture consists of a wedge terminated in a half-cylinder. A one foot by one foot section on one side of the wedge is designed with a recess to accommodate various thicknesses of absorbers. The RCS of different absorbers installed flush to the wedge surface was measured in the plane normal to the axis of the cylinder. The traveling wave/surface wave reflection from the absorbers tested were observed at aspects near edge-on to the wedge. The different absorbers tested are shown in Figure 3-15. The features of each are listed below:

<u>Absorber</u>	<u>Thickness</u>	<u>Type</u>
B-X	0.1	Carbon impregnated rubber - surface wave
CR-124	0.1	Iron impregnated rubber - surface wave
An-74	1.0	Carbon impregnated foam - specular
CA	1.0	Circuit-analog - specular
AN-74 HC	1.0	AN-74 encased in honeycomb core and .020" skin - specular
CR-117	0.1	Iron impregnated rubber - surface wave

(U) The normal incidence and traveling wave absorption (for the absorber as installed in the test fixture) is shown in Figure 3-16 for a 3 GHz frequency. The traveling wave reflection from the wedge with the surface recessed by one inch is the reference (0 db) for the traveling wave reflections. The smooth wedge (zero depth recess) has a reflection about 16 db (a factor of 1/40) below the reflection from the recessed surface. The absorbers all show a larger traveling wave reflection than the smooth wedge. The AN-74HC shows a small reflection compared to the other one inch thick absorbers. This is not the case for similar measurements at higher frequencies. The interaction between the various electromagnetic waves (plane, surface and traveling waves) and the absorber is extremely complex. The scope of this particular program did not provide for the detailed study of absorber installations necessary to positively identify the techniques for designing an appropriate absorber installation. Therefore, it was decided not to pursue the study of the RAM beyond the preliminary level shown here. However, there are techniques for installing absorbers which intuitively should minimize unwanted reflections. The tapering or otherwise shaping of the edges of an absorber installation will definitely affect the surface/traveling wave reflections. The definition of exact designs for minimizing traveling wave and surface wave reflections awaits the development of a more complete understanding of these particular waves. There is no reason to assume that these reflections cannot be minimized in a fashion similar to the specular or plane wave reflections.

UNCLASSIFIED
D180-17939-1



Figure 3-14. Absorber Test Fixture

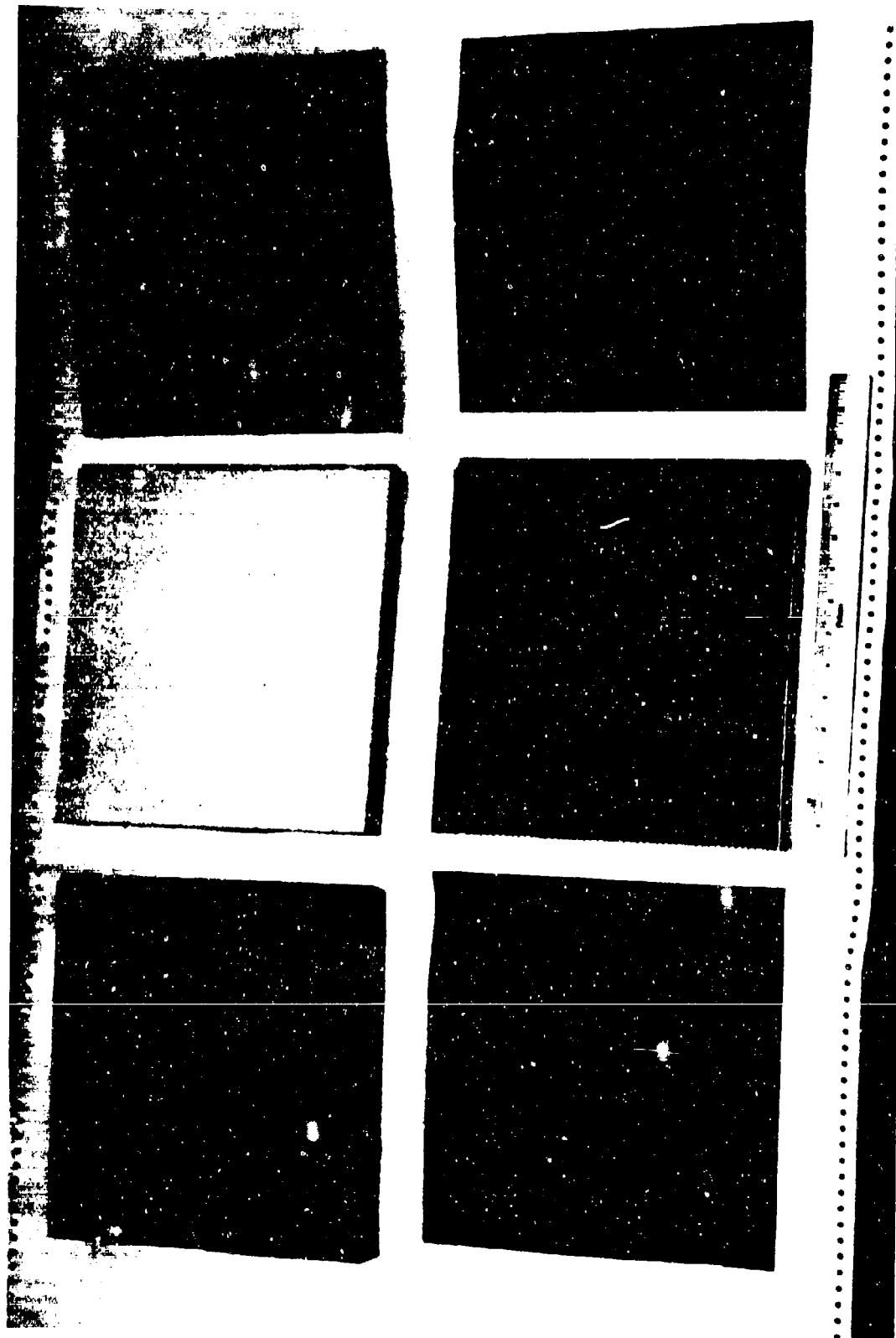


Figure 3-15. Absorber Test Specimens

UNCLASSIFIED

D180-17939-1

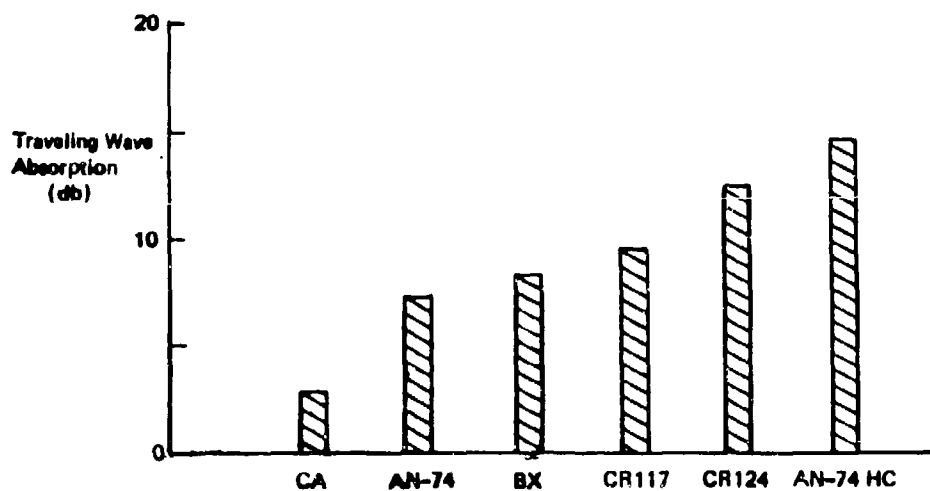
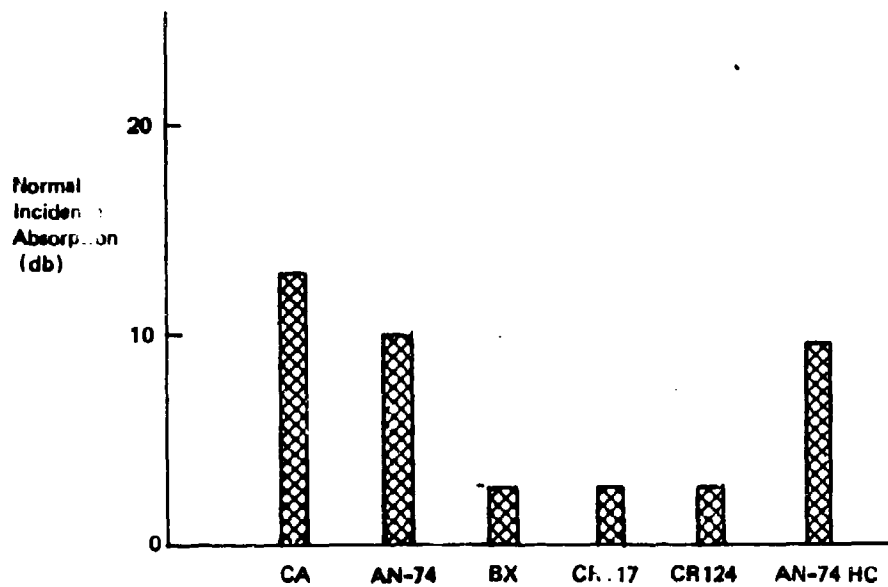
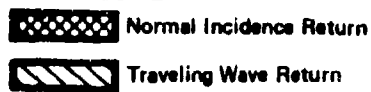


Figure 3.16 : Absorber Performance - 3GHz (U)

UNCLASSIFIED

D180-17939-1

3.2 Design Guideline Data (U)

(U) Four different fuselage shapes are considered along with two wing shapes, three wing locations and three different empennage configurations. The fuselage shapes are circular, triangular, square and elliptical. Subsonic and supersonic wing shapes were considered in low, mid fuselage and high wing locations. The three different tail configurations were the normal T-tail, V-tail and twin tail.

(U) The computer program described in Reference 6 was used to compute the RCS at each point of the broadside sector, for each configuration. The RCS was then averaged over the top sector, i.e. $+30^\circ$ in yaw for roll angles of 0° , $+10^\circ$, $+20^\circ$ and $+30^\circ$, over the bottom sector (roll angles of 0° , -10° , -20° and -30°) and over the whole broadside sector. The results were tabulated and the design guideline data obtained from the tables.

3.2.1 Fuselage Shape (U)

(U) Four different fuselage shapes were considered: circular, triangular, square, and elliptical. The HIPAAS supersonic configuration was used as the baseline aircraft for determining the volume of the various fuselage shapes. The engine inlets were removed and a constant fuselage volume assumed. The body section area of the airplane was measured at each station and converted to the four shapes under consideration. Sharp corners were not allowed for the triangular and square shapes. It was assumed that the edge of the fuselage would have a minimum full scale radius of 5 inches. The triangular and square areas were compensated accordingly to maintain a constant volume fuselage. The canopy was also removed from the HIPAAS airplane in determining the volume of the fuselage shape on the RCS. All of the fuselage RCS computations were made using the "normal" empennage geometry. The normal empennage geometry is a T-tail with a centered vertical stabilizer and two centered horizontal stabilizers (one on each side). To demonstrate the effect of shape, the centered subsonic wing was used with the normal tail, for the four different fuselage shapes. In Figure 3-17, the RCS values (in dbsm) are shown for each of the seven different roll angles of the sector for the circular shaped fuselage. Figures 3-18, 3-19 and 3-20 are the same roll angles for the triangular, square and elliptical fuselage shapes respectively. These results are for a full scale frequency of 4 GHz. The azimuth angles shown are about the aircraft left broadside. Thus, the positive angles are toward the tail and the negative angles are toward the nose. The averages of the RCS values

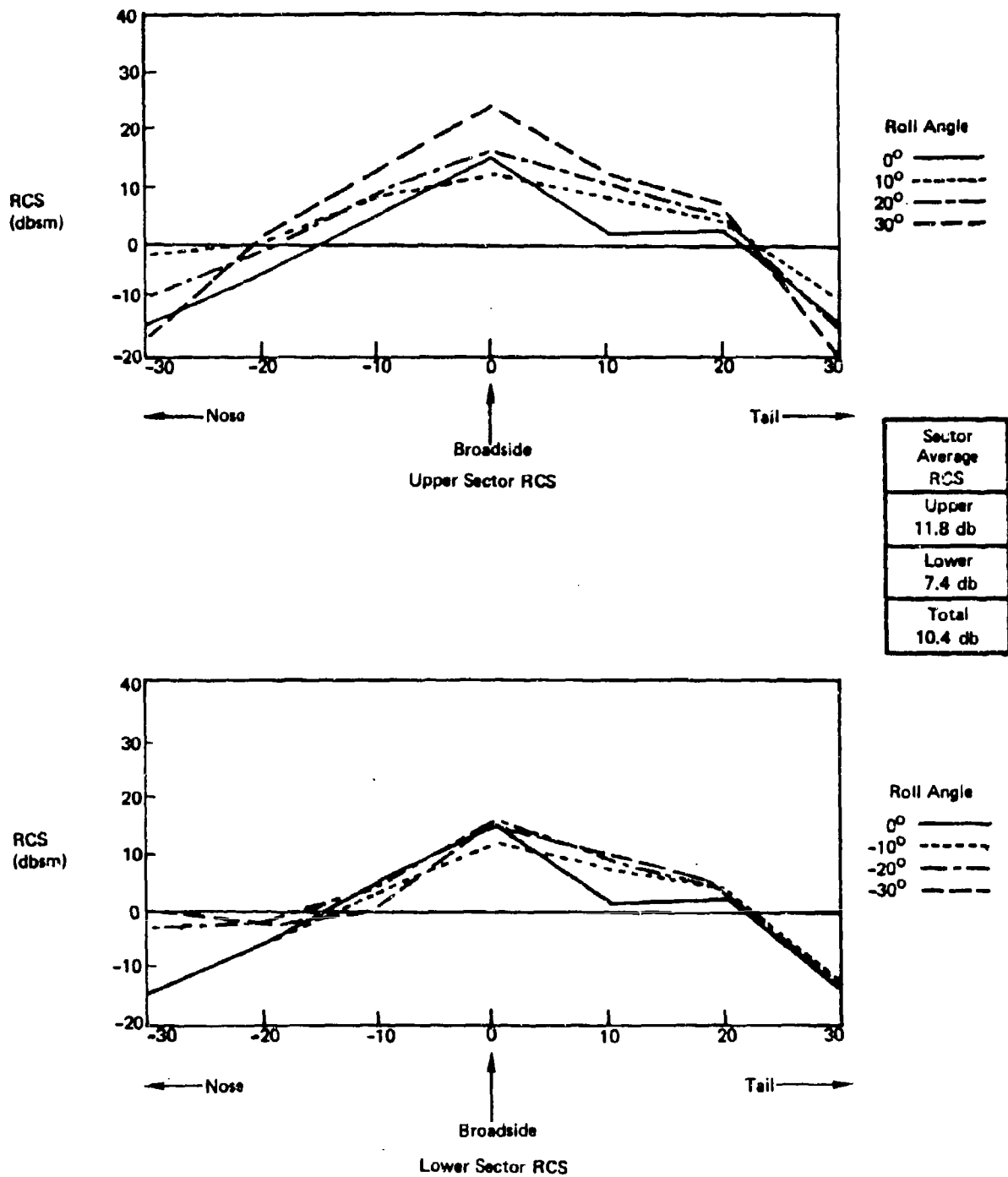


Figure 3.17: Computed RCS - Circular Body - Center Subsonic Wing - 4 GHz (U)

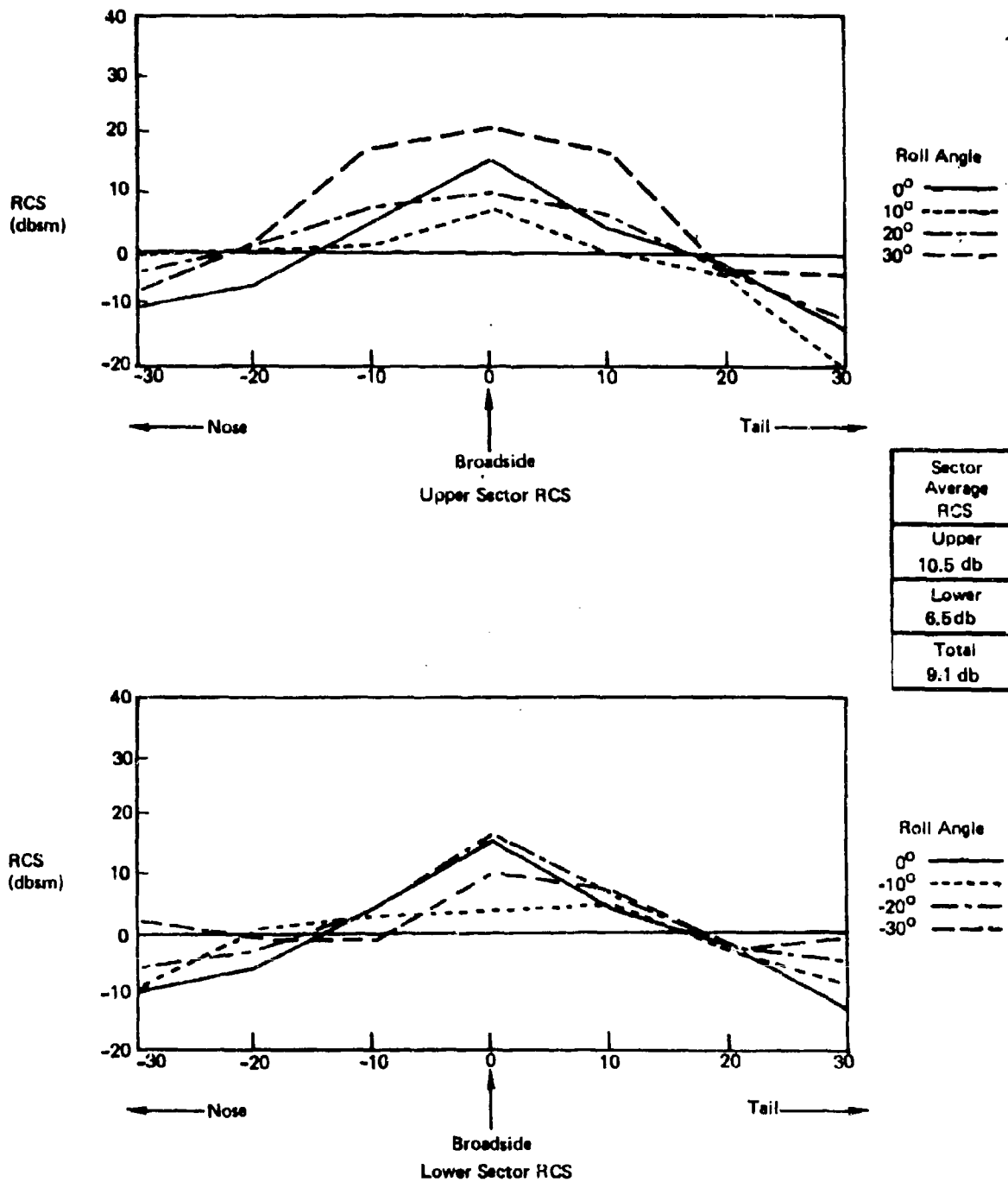


Figure 3.18: Computed RCS - Triangular Body - Center Subsonic Wing - 4 GHz (U)

UNCLASSIFIED

D180-17939-1

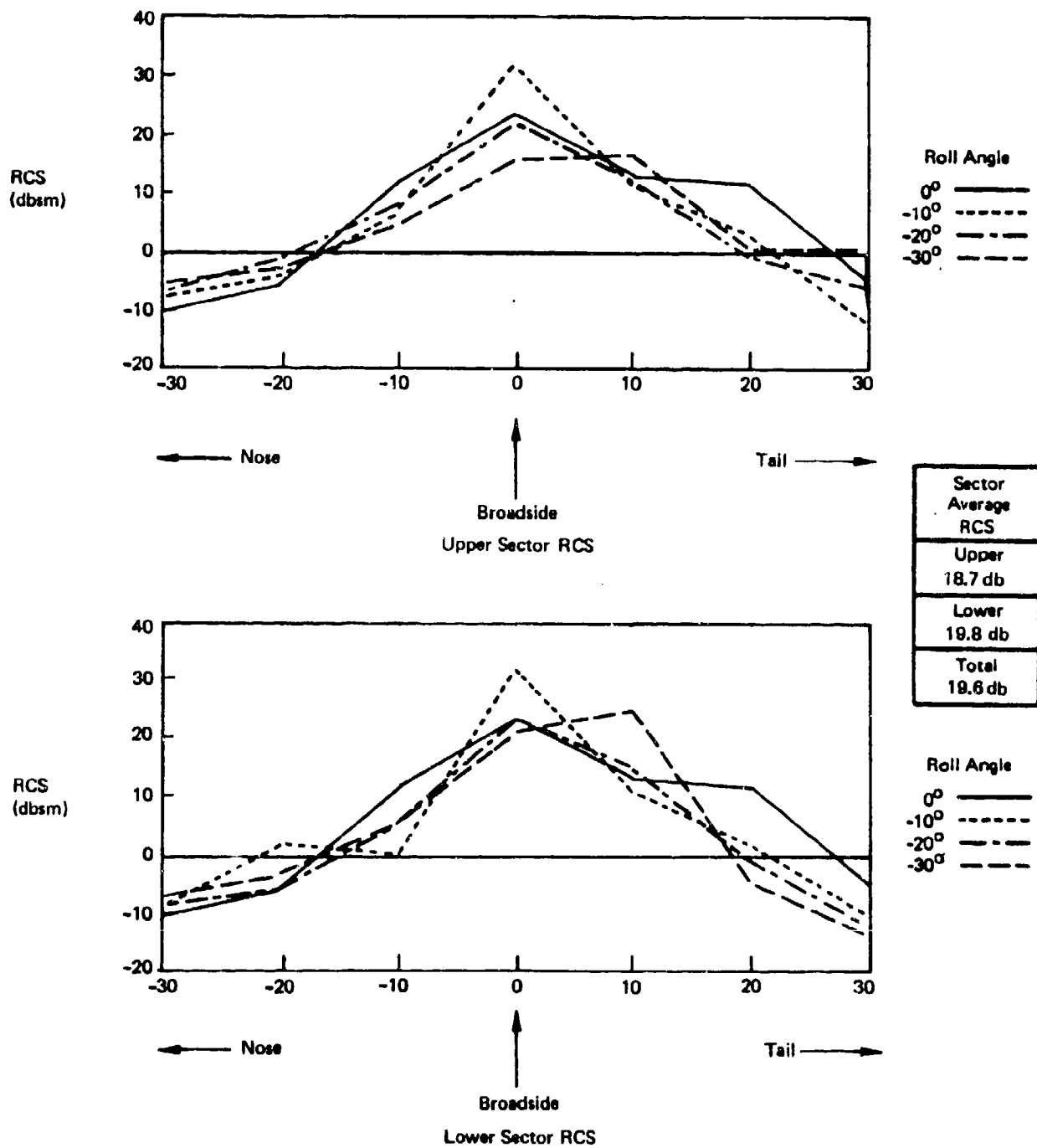


Figure 3.19: Computed RCS - Square Body - Center Subsonic Wing - 4 GHz (U)

UNCLASSIFIED
D180-17939-1

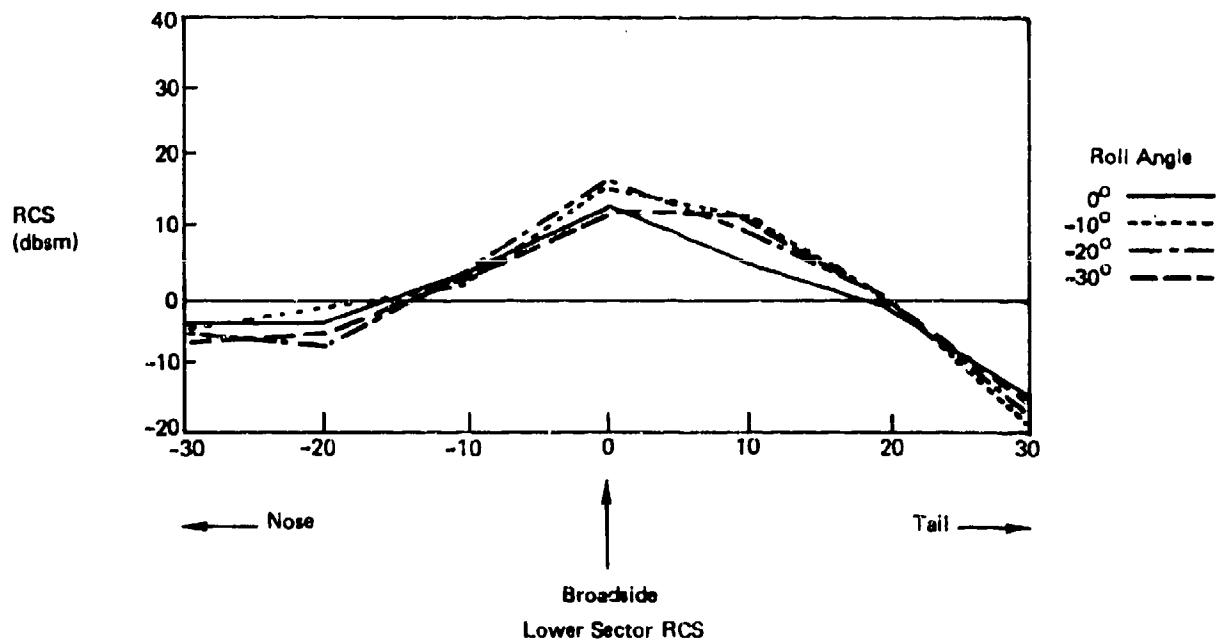
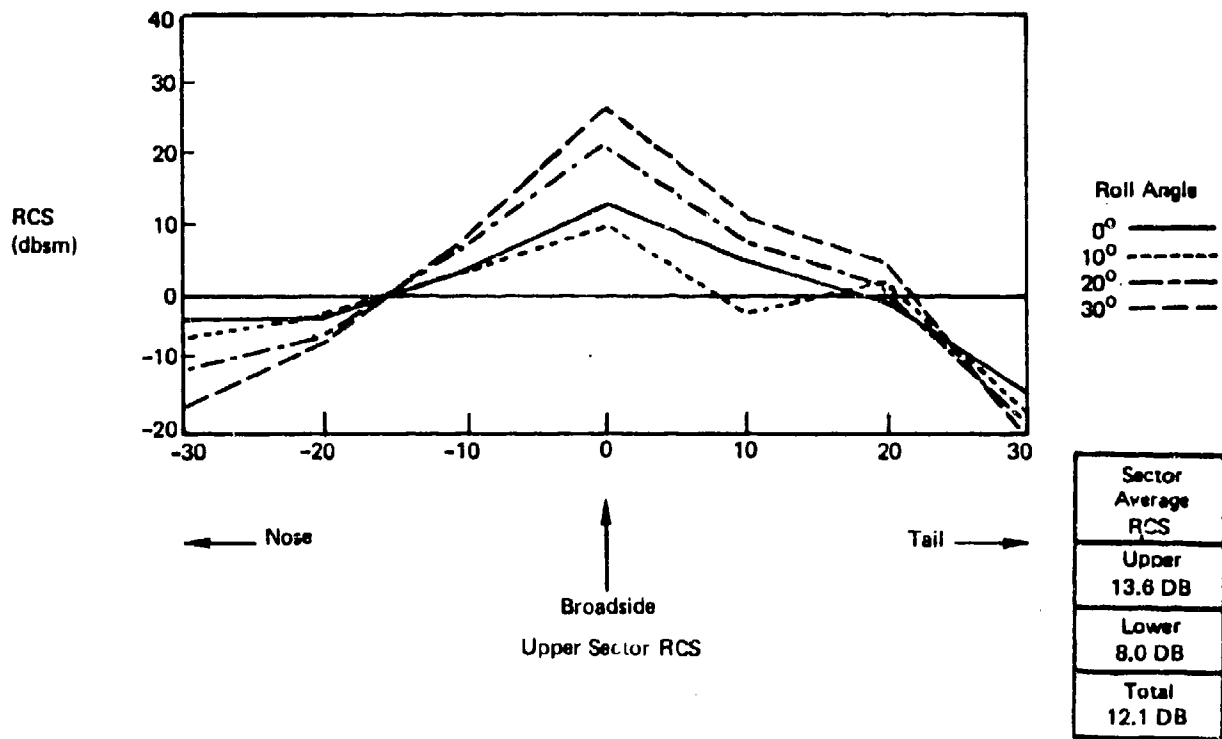


Figure 3.20: Computed RCS - Elliptical Body - Center Subsonic Wing - 4 GHz (U)

UNCLASSIFIED

D180-17939-1

(U) for the top sector (0° , $+10^\circ$ roll, $+20^\circ$ and $+30^\circ$ roll angles) the bottom sector (0° , -10° , -20° and -30° roll) and the whole sector are summarized in Table 3-1 for the centered subsonic configuration, for three full scale frequencies of 2, 4, and 12 GHz.

(U) The change in the average RCS observed at the higher frequency (12 GHz) is contrary to the accepted hypothesis. In general, it is assumed that aircraft RCS is not a function of frequency for large aircraft across the microwave band. However, this assumption is usually applied to the forward and aft sectors where the RCS is comprised of returns from several objects (inlets, antennas, cockpit, etc.). The presence of numerous scatterers separated electrically tends to "smooth" or average any variation due to frequency. The broadside RCS is comprised of returns from discrete regions on the aircraft (fuselage tail, wing) and each discrete scatterer may show a frequency dependence.

3.2.2 Wing Location (U)

(U) The RCS of the broadside sector was determined for three different wing locations. These are bottom, where the bottom of the wing is flush with the bottom of the airplane, centered, where the wing is exactly centered for the circular fuselage, and top where the wing has been moved up as high as possible without having any part above the top line of the airplane. Because the mid body location of the wing was centered based on the circular body configuration, it was found that this location was relatively high on the fuselage for the square and elliptical bodies. Thus for these two configurations, the high wing location did not differ substantially from the center location. Thus calculations were not made of the high wing locations for the square and elliptical bodies.

(U) The wing itself did not have a true airfoil shape. It was made symmetrical (top half to bottom half) for ease of construction of the model used to verify the validity of the computer approach. Typical wing location results are shown in Table 3-2 and 3-3 for the circular and triangular fuselages.

(U) The top wing location, for circular fuselage, has the lowest RCS in the top sector of the broadside area. Similarly in the bottom sector, the bottom wing location has the lower RCS. The center wing location has the lowest RCS when the whole sector is considered.

UNCLASSIFIED
D180-17939-1

TOP SECTOR				
	FUSELAGE SHAPE			
FREQUENCY	CIRCULAR	TRIANGULAR	SQUARE	ELLIPTICAL
2 GHz	13.5	13.6	17.1	14.6
4 GHz	11.8	10.5	18.7	13.6
12 GHz	10.8	5.7	21.4	6.9

BOTTOM SECTOR				
	FUSELAGE SHAPE			
FREQUENCY	CIRCULAR	TRIANGULAR	SQUARE	ELLIPTICAL
2 GHz	9.8	9.4	18.7	9.3
4 GHz	7.4	6.5	19.8	8.0
12 GHz	5.2	4.6	20.9	7.4

ENTIRE SECTOR				
	FUSELAGE SHAPE			
FREQUENCY	CIRCULAR	TRIANGULAR	SQUARE	ELLIPTICAL
2 GHz	11.9	11.9	17.9	12.8
4 GHz	10.4	9.1	19.6	12.1
12 GHz	9.2	5.5	21.7	7.5

(values are in dbsm)

TABLE 3-1 FUSELAGE SHAPE EFFECTS -
CENTERED SUBSONIC WING (U)

UNCLASSIFIED

D180-17939-1

TOP SECTOR			
	SUBSONIC WING LOCATION		
FREQUENCY	CENTER	BOTTOM	TOP
2 GHz	13.5	17.7	14.6
4 GHz	11.8	17.9	10.7
12 GHz	10.8	16.8	6.0

BOTTOM SECTOR			
	SUBSONIC WING LOCATION		
FREQUENCY	CENTER	BOTTOM	TOP
2 GHz	9.8	9.1	14.9
4 GHz	7.9	7.3	16.6
12 GHz	5.2	4.1	17.3

ENTIRE SECTOR			
	SUBSONIC WING LOCATION		
FREQUENCY	CENTER	BOTTOM	TOP
2 GHz	11.9	15.6	15.0
4 GHz	10.4	15.7	15.1
12 GHz	9.2	14.5	15.1

(values are in dbsm)

TABLE 3-2 WING LOCATION EFFECTS -
CIRCULAR FUSELAGE (U)

UNCLASSIFIED

D180-17939-1

TOP SECTOR			
	SUBSONIC WING LOCATION		
FREQUENCY	CENTER	BOTTOM	TOP
2 GHz	13.6	14.3	13.3
4 GHz	10.5	11.2	10.4
12 GHz	5.7	5.3	5.5

BOTTOM SECTOR			
	SUBSONIC WING LOCATION		
FREQUENCY	CENTER	BOTTOM	TOP
2 GHz	9.4	7.8	8.6
4 GHz	6.5	3.2	4.9
12 GHz	1.6	0.1	2.0

ENTIRE SECTOR			
	SUBSONIC WING LOCATION		
FREQUENCY	CENTER	BOTTOM	TOP
2 GHz	11.9	12.1	11.4
4 GHz	9.1	9.0	8.6
12 GHz	5.5	3.7	4.2

(values are in dbsm)

TABLE 3-3 WING LOCATION EFFECTS -
TRIANGULAR FUSELAGE (U)

UNCLASSIFIED

D180-17939-1

(U) The results for the triangular fuselage for each sector show less variation between the top, center and bottom locations than for the circular fuselage. However, the bottom wing location has the largest variation in the bottom sector. The RCS for this configuration is significantly lower than for the center or top wing locations.

3.2.3 Wing Sweep (U)

(U) Two wing sweep angles were investigated for the different fuselage configurations. These were a subsonic wing and a supersonic wing at 20° and 70° from the normal to the broadside, respectively. The wing dimension of the HIPAAS aircraft was used for both shapes. Because of the length of the join between wing and fuselage, it was only possible to determine the RCS of the wing in a top body location for the triangular fuselage. For all other configurations the RCS in the broadside sector was calculated for the center wing and bottom wing locations only.

(U) The RCS results for the triangular fuselage with the two wing sweep angles for the center and bottom wing locations are shown in Tables 3-4 and 3-5.

(U) The RCS is lowest in the bottom sector for both a bottom wing and a centered wing. For the bottom wing location, both subsonic and supersonic wing gives a significantly lower RCS in the bottom sector. The wing sweep study demonstrates that the broadside RCS is generally higher for a supersonic wing. However, the RCS can be controlled at a lower level by choosing a wing fuselage join which permits very little corner reflection effect, as in the triangular fuselage case.

3.2.4 Empennage Shape (U)

(U) Three different empennage shapes were studied to show the effect on the broadside sector RCS. The circular body with the centered subsonic wing was used as the basis for the study and the different empennages added. The normal tail assembly is the T-tail with a centered vertical and centered horizontal stabilizers at the rear of the fuselage. The V-tail has only two stabilizers extending from the center rear of the fuselage up and out each side of the aircraft at a 45° angle from the horizontal. The twin tail has the same horizontal stabilizers as the normal tail. The two vertical stabilizers are about 15% smaller than the normal tail, and are located above the horizontal stabilizer and flush with the edge of the fuselage. The tops are tilted in toward the

UNCLASSIFIED

D180-17939-1

TOP SECTOR		
	WING SWEEP - TRIANGULAR BODY	
FREQUENCY	SUPERSONIC WING	SUBSONIC WING
2 GHz	14.7	13.6
4 GHz	14.5	10.5
12 GHz	21.5	5.7

BOTTOM SECTOR		
	WING SWEEP - TRIANGULAR BODY	
FREQUENCY	SUPERSONIC WING	SUBSONIC WING
2 GHz	9.5	9.4
4 GHz	7.2	6.5
12 GHz	8.1	4.6

ENTIRE SECTOR		
	WING SWEEP - TRIANGULAR BODY	
FREQUENCY	SUPERSONIC WING	SUBSONIC WING
2 GHz	12.8	11.9
4 GHz	12.6	9.1
12 GHz	19.3	5.5

(values are in dbsm)

TABLE 3-4 WING SWEEP EFFECTS -
CENTER LOCATION (U)

UNCLASSIFIED

D180-17939-1

TOP SECTOR		
	WING SWEEP - TRIANGULAR BODY	
FREQUENCY	SUPERSONIC WING	SUBSONIC WING
2 GHz	14.5	14.3
4 GHz	12.0	11.2
12 GHz	5.3	5.3

BOTTOM SECTOR		
	WING SWEEP - TRIANGULAR BODY	
FREQUENCY	SUPERSONIC WING	SUBSONIC WING
2 GHz	8.4	7.8
4 GHz	4.7	3.2
12 GHz	1.4	0.1

ENTIRE SECTOR		
	WING SWEEP - TRIANGULAR BODY	
FREQUENCY	SUPERSONIC WING	SUBSONIC WING
2 GHz	12.4	12.1
4 GHz	9.9	9.0
12 GHz	3.9	3.7

(values are in dbsm)

TABLE 3-5 WING SWEEP EFFECTS -
BOTTOM LOCATION (U)

UNCLASSIFIED

D180-17939-1

(U) center at an angle of 15° . The results of the broadside RCS for the empennage assemblies are given in Table 3-6.

(U) The normal tail has the highest RCS levels due to the scattering from the large vertical stabilizer. The V-tail contributes the smallest RCS in the broadside because in this sector, there is little geometric optics scattering from this empennage configuration.

(U) The twin tail has a smaller broadside RCS than the normal because of the smaller size of the vertical stabilizer than the normal tail. From a strictly RCS viewpoint, and considering only the broadside sector, the V-tail is the preferred empennage configuration.

UNCLASSIFIED

D180-17939-1

TOP SECTOR			
	EMPENNAGE		
FREQUENCY	SINGLE TAIL	V-TAIL	TWIN TAIL
2 GHz	13.5	7.4	10.1
4 GHz	11.8	6.8	8.1
12 GHz	10.8	5.5	6.9

BOTTOM SECTOR			
	EMPENNAGE		
FREQUENCY	SINGLE TAIL	V-TAIL	TWIN TAIL
2 GHz	9.8	8.5	8.4
4 GHz	7.4	7.6	7.1
12 GHz	5.2	3.1	5.7

ENTIRE SECTOR			
	EMPENNAGE		
FREQUENCY	SINGLE TAIL	V-TAIL	TWIN TAIL
2 GHz	11.9	8.2	9.7
4 GHz	10.4	7.4	8.0
12 GHz	9.2	4.8	6.7

(values are in dbsm)

TABLE 3-6 EMPENNAGE EFFECTS (U)

UNCLASSIFIED

D180-17939-1

4.0 DESIGN GUIDELINE APPLICATION (U)

(U) All available RCS data was used to design a fighter attack aircraft which would have a low RCS signature - especially in the broadside sector. A model of the proposed aircraft was built and the RCS measured on the range.

4.1 Low RCS Aircraft Design Selection (U)

(U) In designing the low RCS aircraft for this study, the basic purpose was to have an aerodynamically stable, high performance aircraft with a low RCS in the lower sector (0° to 30° below the yaw plane). The results, summarized in Table 3-1, indicate that a triangular fuselage has the lowest RCS in the bottom broadside sector for both subsonic and supersonic wings. The wing location studies tabulated in Table 3-2 and the Summary indicate that the low wing location results in the lowest RCS in the broadside sector. The study on fairings in Figures 3.8 and 3.9 demonstrate that it is desirable to fair the wings into the fuselage to maintain a low RCS. From the results in Table 3-6, the V-tail gives the lowest RCS in the broadside sector. However, the stability and control problems associated with a V-tail were sufficient to offset the RCS advantages. Therefore, the twin tail was selected. This empennage is only slightly higher in RCS and substantially superior from a flight dynamics viewpoint.

(U) The aircraft configured from the above design data is very similar to the aircraft previously proposed as a "Low RCS" fighter-attack aircraft. Only minor modifications were required based on the design guidelines developed during this study.

(U) The fairings between the wing and fuselage and the empennage and fuselage, were the major configuration details changed from the previous "Low RCS Airplane" configuration. These fairings are critical to the control of the traveling wave reflections.

4.2 "Low RCS Airplane" Model Tests (U)

(U) The one-eighth scale model of the "Low RCS Airplane" configuration, shown in Figure 4.1 was tested on the RCS range to establish the broadside sector RCS. The model RCS was measured at 33 GHz corresponding to a 4.125 GHz full scale frequency. RCS data was taken at vertical and horizontal polarizations at model roll angles of $+30^\circ$, $+20^\circ$,

UNCLASSIFIED

D180-17939-1



Figure 4.1: Low RCS Airplane (U)

~~SECRET~~

DL80-17939-1

(U) $+10^{\circ}$, 0° , -10° , -20° , and -30° . The measured RCS was recorded on a magnetic tape in digital form at every 0.1° interval. The resulting digital data was subsequently computer processed to establish the median RCS over each ten degree interval and the average of the medians over the entire broadside sector as well as the upper (0° to $+30^{\circ}$ roll) and lower (0° to -30° roll) sectors.

(U) The resulting median RCS is shown in Figure 4.2 and Figure 4.3 for vertical and horizontal polarizations, respectively. The median averages for the three sectors were also computed and are shown on the figures.

(S) The lower broadside sector was defined to be the sector of major emphasis for RCS control for this airplane. The goal was to keep the sector average below ten square meters full scale. The ten degree median RCS derived from the measurements does not exceed ten square meters at any point in the lower sector. The averages of the 10° median RCS over the lower sector are 3.5 dbsm (2.2 m^2) and 3.2 dbsm (2.1 m^2) and 3.2 dbsm (2.1 m^2) at vertical and horizontal polarization, respectively. These levels are well below the RCS of a "conventional" aircraft. Broadside RCS levels are typically on the order of several hundred square meters for conventional aircraft.

(S) Contour plots of the RCS in the broadside sector were produced by plotting the seven different roll angle RCS curves on a three dimensional grid. The results are shown in Figure 4-4 for vertical polarization and Figure 4-5 for horizontal polarization. The peak of the horizontal polarization is much broader than that for vertical polarization. The RCS is below the 10 dbsm (10 square meters) contour in the entire lower sector. The RCS exceeds 5 dbsm ($3.2 \text{ square meters}$) for only a small part of the lower sector. A RCS distribution such as this is extremely desirable from an ECM viewpoint. Inasmuch as the RCS is fairly low (below 10 square meters), and also confined to a singular "lobe" it is possible to consider an ECM system which has simple fixed beam antennas. This type of ECM system does not require complex scanning and direction finding equipment. The aircraft can, therefore, be effectively screened with a minimal cost and higher reliability due to the lower RCS. This will provide for increased survivability against advanced threats with a broadside shot capability.

~~SECRET~~

UNCLASSIFIED

D180-17939-1

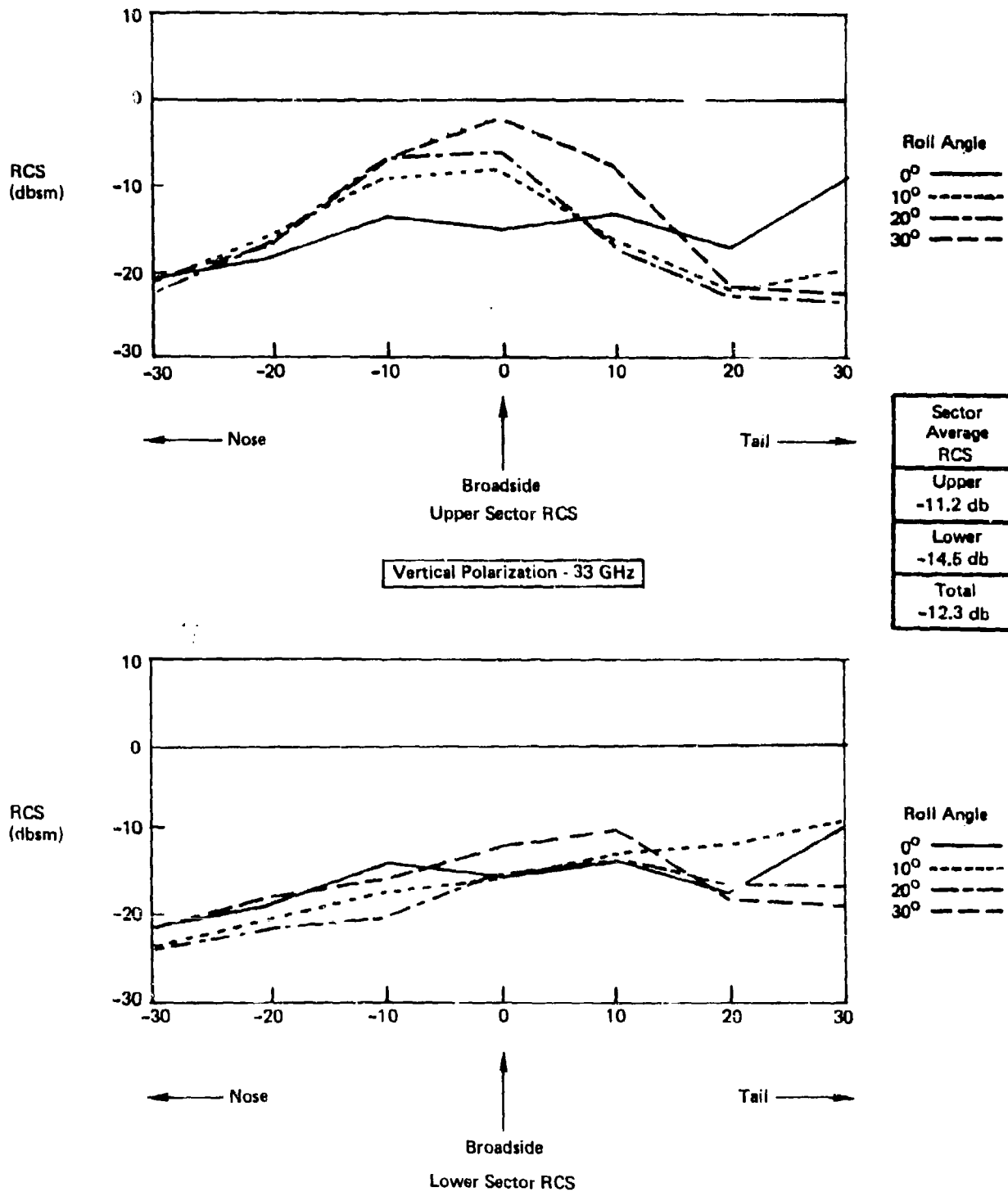


Figure 4-2: Measured RCS - Low RCS Airplane (U)

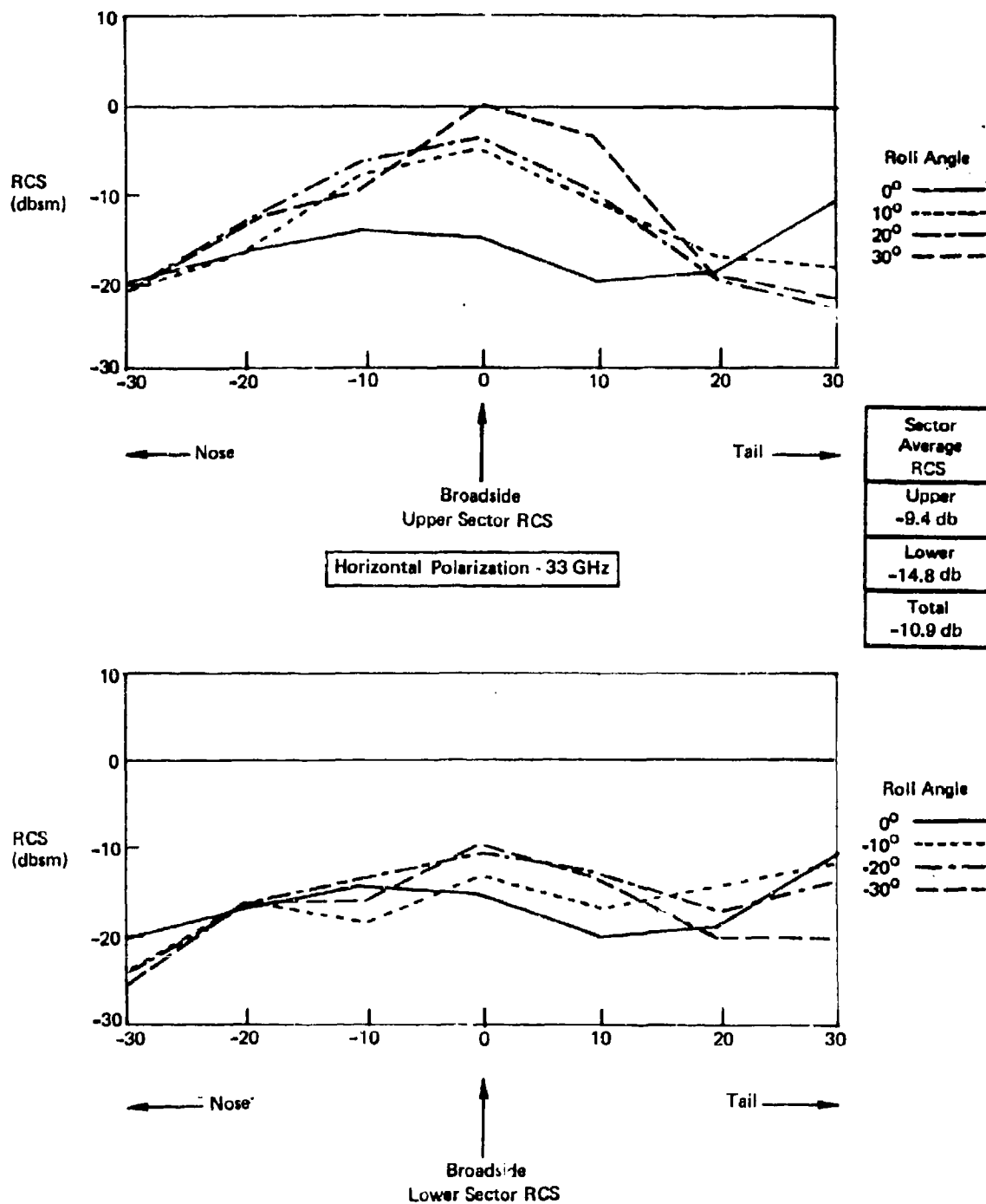


Figure 4-3: Measured RCS - Low RCS Airplane Model (U)

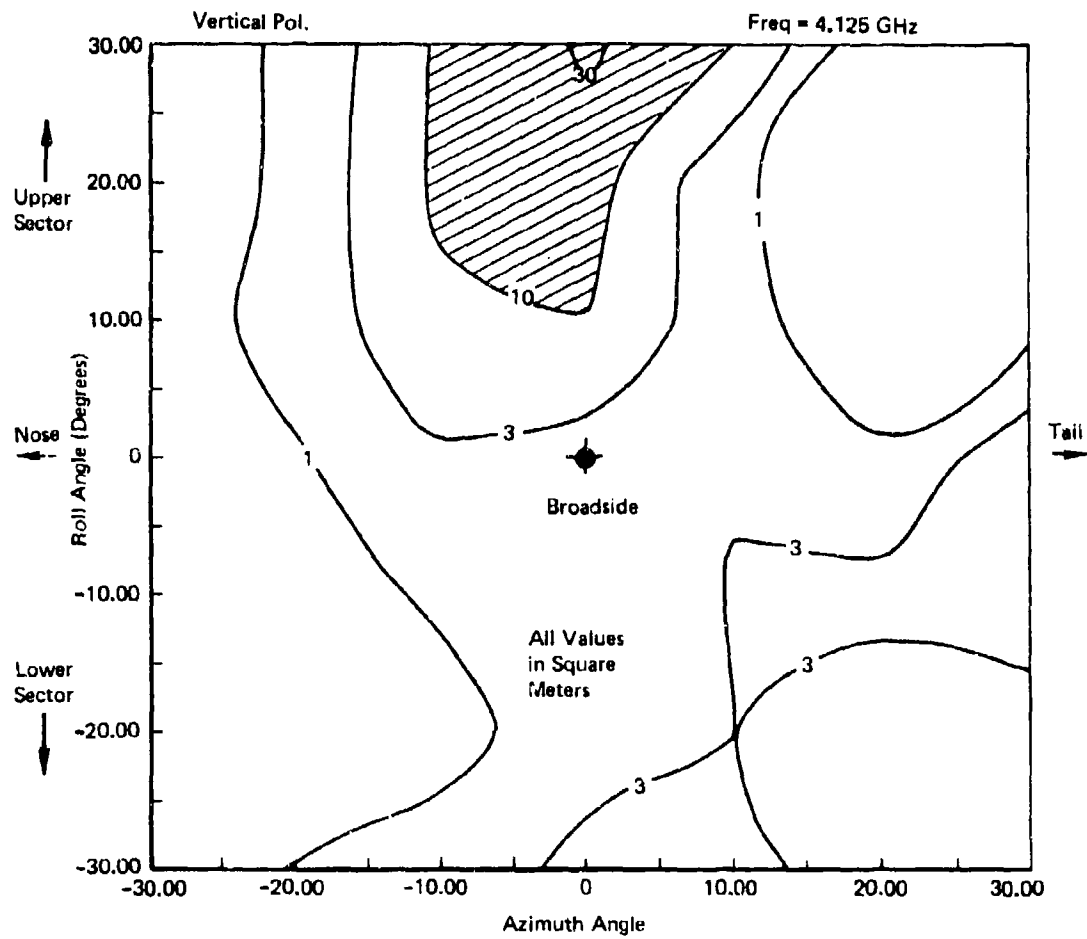


Figure 4.4 : RCS Contours - Low RCS Airplane (U)

UNCLASSIFIED

D180-17939-1

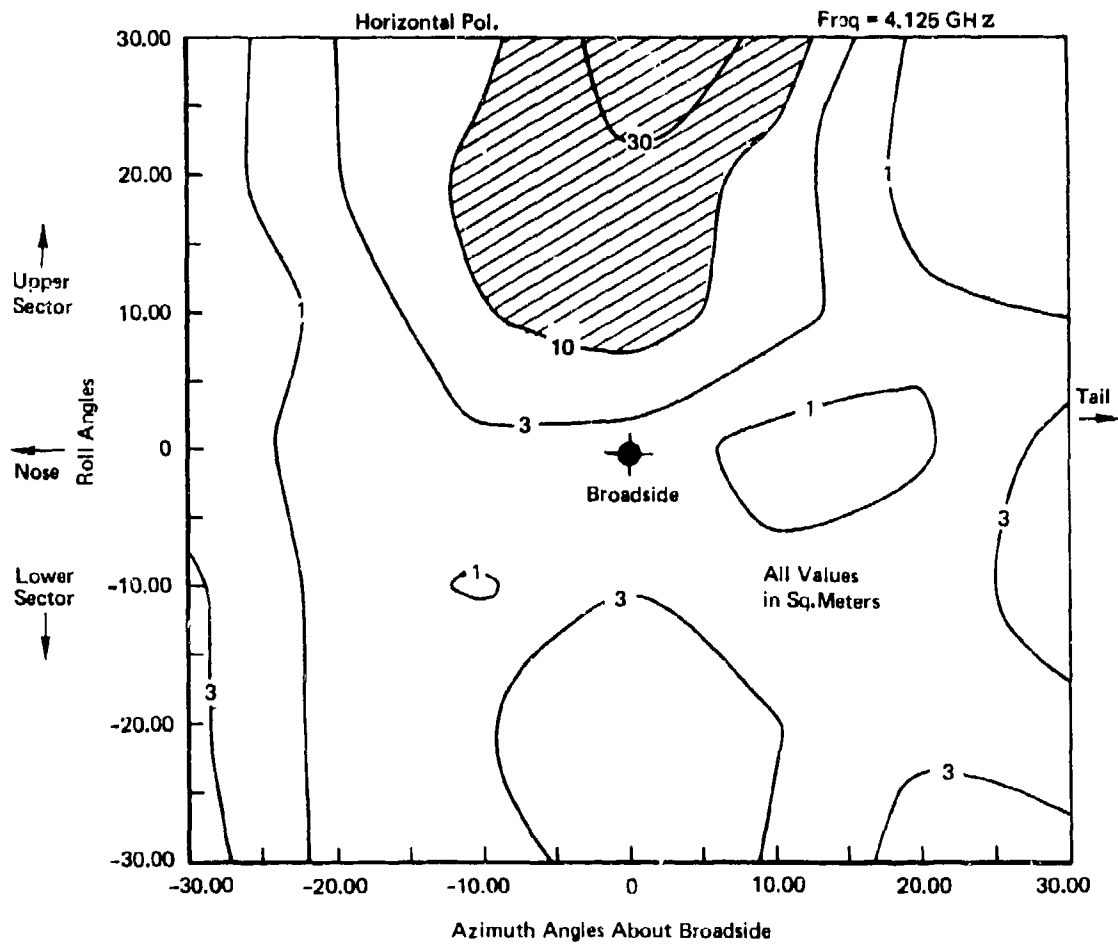


Figure 4.5 : RCS Contours - Low RCS Airplane (U)

~~SECRET~~

D180-17939-1

5.0 CONCLUSIONS AND RECOMMENDATIONS (U)

(S) The results of this study have established several conclusions relative to aircraft RCS over the broadside sector.

1. A substantial control of aircraft RCS over the broadside sector is possible by careful configuration selection.
2. Broadside RCS can be held to below ten square meters throughout the majority of the broadside sector.
3. Traveling wave reflections can exceed 100 square meters peak and can average near 1 square meter over the entire broadside sector.
4. Traveling wave reflections can be effectively reduced by careful fairing of all abrupt surface discontinuities.

(U) This study has demonstrated the practical aspects and feasibility of design of aircraft for low RCS over the broadside sector. The reduction of the RCS controls to practice will require some additional research. Recommended items for additional study include:

1. A rigorous analytical description of the propagation and reflection of traveling waves and surface waves.
2. Techniques for the control of traveling waves and surface waves.
3. Effects of wing and fuselage surface roughness and irregularities on RCS.
4. The quantitative benefits to weapon system cost, survivability, maintenance, reliability and other system parameters due to RCS control should be determined for a selected aircraft.

(U) Item four above is of particular importance since payoffs must be demonstrated before RCS controls will be seriously considered in a weapon system design. The payoffs to an aircraft system depend on the particular system, the threats and the ECM environment. Therefore, the payoffs derived from RCS control must be assessed for each individual system. The RCS controls demonstrated for the "Low RCS Aircraft" of this study would provide a good basis for a payoff study around some scenario of interest to the Navy. The results

~~SECRET~~

UNCLASSIFIED

D180-17939-1

(U) of this payoff study would clearly demonstrate the numerous system benefits for one advanced weapon system. The payoffs associated with RCS control have been alluded to previously. The few attempts to qualify some of these payoffs have shown that system cost savings or survivability improvements can be realized by control of RCS. However, these attempts have not been either thorough enough or specific enough to firmly identify RCS payoffs.

UNCLASSIFIED

UNCLASSIFIED

D180-17939-1

6.0 REFERENCES (U)

1. D180-14192-1, Design of Naval Fighter-Attack Aircraft for Low RCS, January 1972, The Boeing Company, Secret.
2. D180-15330-1, Design of Aircraft Control Surfaces Low Radar Cross Section, May 1973, The Boeing Company, Secret.
3. AD515252, Evaluation of the Effectiveness of Radar Cross Section Reduction as a Penetration Aid, May 1971, Cornell Aeronautical Laboratory, Secret.
4. Barlow H.M., and Brown J. "Radio Surface Waves", Clarendon Press, 1962.
5. Collin R.E., and Zucker F.J., "Antenna Theory Part 2" McGraw-Hill, 1969.
6. Howell N.A., and Tsiang G.S., "Electromagnetic Scattering Prediction by Computerized Ray Optics" URSI Symposium on Electromagnetic Waves, 24-29, June 1968, Stresa, Italy.

UNCLASSIFIED

D180-17939-1

Distribution List

Office of Naval Research
Department of the Navy
Arlington, Virginia 22217
ATTN: D. S. Siegel, Code 411 (4)

Director
U.S. Naval Research Laboratory
Washington, D.C. 20390
ATTN: Code 5340 (1)
Tech Info Division (1)
Code 5705(c) (1)

Chief of Naval Operations
Washington, D.C. 20350
ATTN: NOP-982E2 (1)

Chief of Naval Material
Washington, D.C. 20360
ATTN: NMAT 0334 (1)

Commander
Naval Air Systems Command
Washington, D.C. 20361
ATTN: NAVAIR 310B (1)
NAVAIR 320A (1)
NAVAIR 320B (1)
NAVAIR 360 (1)
NAVAIR 370S (1)
NAVAIR 510A3 (1)
NAVAIR 52033B (1)
NAVAIR 53364D (1)

Director
Office of Naval Research Branch Office
1030 East Green Street
Pasadena, California 91101
ATTN: CDR R. L. Breken (1)
Mr. R. F. Lawson (1)

Commander
Naval Weapons Center
China Lake, CA 93555
ATTN: Mr. F. Ashbrook, Code 35 (1)
Mr. G. Handler, Code 35034 (1)
Mr. G. Hollingsworth (1)

UNCLASSIFIED

D180-17939-1

Distribution List Cont.

Commander
Naval Air Development Center
Warminster, PA 18974
ATTN: Mr. G. Marsh, Code 30-5 (1)
Mr. J. F. Guarini, Code 2041 (1)
Mr. Robert E. Lee, Code 2041 (1)
Mr. L. Rakszawski, Code 2043 (1)

Commander
Naval Missile Center
Pt. Mugu, CA 93042
ATTN: Mr. F. Miley, Code 5351 (1)
Mr. E. Harris, Code 5365 (1)

Air Force Flight Dynamics Laboratory
(AFSC)
Wright Patterson AFB, OH 45433
ATTN: Mr. P. Baxter, PTS (1)
Mr. D. Fearnow, PTS (1)
Mr. C. Patterson, PTR (1)
Mr. John Seaberg, PTR (1)
Mr. D. W. Voyles, FBS (1)

Air Force Avionics Lab
(AFSC)
Wright Patterson AFB, OH 45433
ATTN: Mr. W. Bahret, WRP (1)
Mr. T. Madden, WRD (1)
Mr. R. Symonds, WRP (1)

Air Force Materials Laboratory
(AFSC)
Wright Patterson AFB, OH 45433
ATTN: Mr. M. J. Foreman (1)
Mr. S. Litvak, LTF (1)
Mr. T. Reinhart, LAE (1)
Mr. R. Van Vliet, LPT (1)

Aeronautical Systems Division
(AFSC)
Wright Patterson AFB, OH 45433
ATTN: Mr. J. T. Bradley, ENVEC (1)
Dr. S. Zakanycz, XRHD (1)

UNCLASSIFIED

DL80-17939-1

Distribution List Cont.

Rome Air Development Center AFSC
Griffiss Air Force Base
Rome, NY 13440
ATTN: Mr. Robert Ragazzo, RADC/IRAP (1)

Headquarters
U.S. Air Force
Washington, D.C. 20330
ATTN: AFRDRE (1)

Air Force Systems Command
Andrews AFB, MD
ATTN: Mr. P. L. Sandler, Code DLCA (1)

U.S. Army Air Mobility R&D
Laboratories, Eustis Directorate
Fort Eustis, VA 23604
ATTN: Mr. J. K. Ladd, SAVLL-EU-SS (1)

Army Materiel Systems Analysis Agency
Aberdeen Proving Ground, MD 21005
ATTN: Mr. W. Paris, AMXSY-AAS (1)

U.S. Army Electronics Command
Fort Monmouth, NJ 07703
ATTN: Mr. R. Giordano, AMSEL-WL-N (1)

U.S. Army Aviation Systems Command
P. O. Box 209
St. Louis, MO 63166
ATTN: Capt. David Linder, AMCPM-IRCM (1)

Defense Documentation Center
Cameron Station, Building 5
5010 Duke Street
Alexandria, Virginia 22314 (2)